STEREOSELECTIVITY IN ORGANOMETALLIC CATALYSIS: ANALYSIS BY MEANS OF COMPUTATIONAL AND MATHEMATICAL CHEMISTRY

Glenn R. Morello

A Thesis Submitted to the
University of North Carolina at Wilmington in Partial Fulfillment
Of the Requirements for the Degree of
Master of Science

Department of Chemistry

University of North Carolina at Wilmington

2003

Approved by

Advisory committee

_____ _____

_____ _____

_____
Chair

Accepted by

_____
Dean, Graduate School

TABLE OF CONTENTS

ABSTRACT

Understanding stereoselective binding of chiral organometallic complexes is essential to control the production of a desired stereoisomer. Computational methods are useful predictors of stereoisomers if all conformations that can participate in a reaction are identified. This thesis introduces new strategies for producing and analyzing conformational search data of organometallic complexes, specifically the chirally pure, coordinatively unsaturated $[(\eta^5\text{-}C_5R_5)Re(NO)(L)]^+$ fragment (R = H and Me, L = PPh_3 and PMe_3), and chiral diphosphine Rhodium(I) catalyst precursors. A new program, cClus-A, is also introduced to examine conformational clusters of the Rhenium systems and for the Rhodium catalyst precursors.

cClus-A was tested rigorously on systems containing 2 torsion angles (Rhenium system), and systems that contain 4 torsion angles (Rhodium complexes). Results of the cClus-A show that in both systems more than one conformation exists near the global minimum that can participate in a stereoselective reaction. When compared with literature values of calculated diastereoselectivity, the new techniques put forth in this thesis show exceptional agreement.

ACKNOWLEDGMENTS

Thanks go to *aaiPharma* for their generosity to allow me to chase my goals while maintaining a steady position where my newfound knowledge will help towards company growth. Especially to Dr. David White for keeping my head on straight in times of doubt and continuing to mentor me through his transition of jobs.

Special thanks to my family and friends for giving me my freedom, without too much guilt, during a very busy time, where school and work made me somewhat invisible to them. All of my love goes to them.

Also thanks to the North Carolina Supercomputing Center for providing me with an extension in computational time, without which I would not have been able to finish this thesis. Without Lee Bartolotti at NCSC, problems I encountered that would have been speed bumps on the road to finishing my research, but instead were smoothed out.

To the University of North Carolina at Wilmington for the resources and excellent faculty present, allowing me to use Chemical and Mathematical departments to combine research interests in order to develop *"de novo"* applications and ideas.

DEDICATION

I would like to dedicate this thesis to my cat Harmony who suffered the greatest neglect in the form of back rubs while I engulfed myself in research on the computer.

LIST OF TABLES

LIST OF FIGURES

CHAPTER 1. CONFORMATIONAL ANALYSIS

Determination of all conformational degrees of freedom, although a routine task in computational organic chemistry, is extremely challenging in computational inorganic and organometallic chemistry. This challenge is a consequence of the chemical diversity of the transition metals, which presents a difficulty in determining a single set of general rules upon which to conduct a conformational search. There are four manifestations of chemical diversity that must be considered in any computational method that claims to thoroughly search conformational space:

i. coordination number and geometry,

ii. isomers,

iii. fluxionality, and

iv. chelate ring inversions.

Structural diversity of transition metal complexes manifests itself in the combination of coordination number and geometry for a single metal ion. For example, five coordinate geometries are known to be either square pyramidal or trigonal bipyramidal. Furthermore, distorted geometries, due to the electronic nature of the metal complex, are also known, for example the ubiquitous distorted tetragonal geometries exhibited for copper(II) coordination complexes. However, the degree of distortion from a regular octahedron is difficult to predict. Certain metal ions can adopt different coordination numbers depending on the oxidation state. For example,

cobalt(II) complexes are predominantly tetrahedral and octahedral whereas cobalt(III) complexes are almost exclusively octahedral.[1] To complicate matters further, cobalt(II) complexes can also have trigonal, square planar, trigonal bipyramidal, square pyramidal, and dodecahedral geometries.[1]

It has been seen in the literature that there are several different types of "isomers" that are possible for transition metal containing complexes:

(i) structural isomers (see above),

(ii) geometric isomers (e.g., *mer* versus *fac* for octahedral complexes),

(iii) coordination isomers (e.g., *axial* versus *equatorial* for trigonal bipyramidal complexes),

(iv) linkage isomers (e.g., cyanide versus isocyanide), and

(v) spin "isomers" (typically for open shell $d^{3\text{-}7}$ metal ions).

To date (i) and (v) have been discussed in the literature.[2,3]

Several organometallic molecules can exhibit fluxional behavior. For example, triginal bipyramidal complexes are known to undergo rapid *axial* / *equatorial* isomerization at room temperature.[1] Another example of fluxionality in the organometallic arena is the migration of metals about a cyclopentadienyl ring in (η^1-C_5H_5) complexes (Figure 1).[4] Where fluxional behavior exists, the computational chemist must either model an averaged structure, which would exist under ambient conditions, or attempt to model each one of the individual structures that can exist.

Finally, chelate rings in coordination complexes are known to undergo rapid δ to λ transition (Figure 2).[5] It is possible that one of the two chelate ring conformations is more stable than the other. If there is a small energy difference between the conformers, then both must be modeled. However, when a large energy difference exists between the conformers, only the lowest energy one needs to be modeled. To complicate matters further, the chelate ring conformation that exists experimentally may not be known *a priori*, in which case all possible chelate ring conformations should to be modeled.

In computational chemistry, there are three accepted approaches to generate a conformational space for a molecule:

i. grid or systematic searches,

ii. stochastic, random, or Monte Carlo methods, and

iii. applications of molecular dynamics.

For molecules with only one rotatable bond, a grid search incrementally rotates that bond and optimizes the structure after each rotation. When there is more than one rotatable bond in the molecule, each torsion angle is adjusted as a function of all the others. Consequently, if the user-defined increment is fine enough, then we are guaranteed of locating the global minimum in the torsional space of the molecule. However, in order to obtain a fine enough grid, a very large number of structures must be generated for molecules with more than two rotatable bonds. Therefore, stochastic methods are generally considered.

Most stochastic conformational search methods employ a variation of the Monte Carlo algorithm. For example, each rotatable bond in the molecule is randomly assigned a different torsion angle and then the geometry of the structure is optimized. The user determines the total number of daughter structures to be generated. Consequently, there is no guarantee of obtaining the global minimum by the use of stochastic methods, but there is the guarantee that the conformational search algorithm will terminate in a reasonable amount of time. One limitation of both the grid and stochastic searches as described is that generally torsion angles that are part of a ring, either carbocyclic or chelate, are not adjusted.

An alternative conformational search strategy is the random jump method, in which all the atoms in the molecule are assigned random Cartesian coordinates, while maintaining connectivity, and the structure is then geometry optimized. One potential problem with the random jump methodology is that the structure can become grotesquely distorted, which makes geometry optimization intractable.

The conformational space of metals that are part of chelate ring systems is particularly difficult to sample and, to our knowledge, LIGB is the only stochastic search that is capable of changing chelate ring conformation.[2] During a LIGB search, all "ligand bonds", designated by the user, are broken and all torsion angles in the molecule, including those generated by the broken bonds, are rotated by randomly different amounts.[2] Prior to geometry

optimization, the ligand bonds are re-attached. Combination of LIGB and high-temperature molecular dynamics is an efficient method for searching the conformational space of a transition metal containing complex.

Low-temperature molecular dynamics (LTMD, temperatures around 500 K) is frequently used to refine a minimum. If the potential energy surface of a molecule contains several minima of similar energies separated by low energy barriers, then LTMD will locate the lowest energy minimum. High temperature molecular dynamics, HTMD (T > 750 K), on the other hand will provide the system with sufficient energy to rotate phenyl rings, for example. Workers have shown that a combination of LIGB and HTMD is a good strategy to locate important minima in organometallic complexes.[2] Other workers have indicated that a combination of stochastic conformational search and LTMD provides a good representation of the lowest energy structure for a complex.[6-9] Most conformational searches on organometallic complexes are carried out with molecular mechanics because of the relatively large number of basis functions and the number of structures that need to be generated to adequately sample the conformational space. Steric effects are well represented in MM,[10] so the conformational search results are a good indication of the steric map of metal containing complexes.

There are three levels of computational theory that are used to generate a conformational space for a molecule: molecular mechanics (MM), semiempirical quantum mechanics (SEQM), and quantum mechanical (QM)

methods, of which density functional theory (DFT) predominates in organometallic chemistry.

It has been recently noted that optimal ligand design requires the use of many levels of computational theory rather than the traditional approach of using just one level of theory for a given problem.[2,3] Each computational level of theory provides a more sophisticated refinement than its predecessor. In this, so called, *de novo* design approach, each successive methodology is increasingly computationally expensive from MM through SEQM to DFT. Because of this increase in computation time, fewer structures can be submitted at each successive level of theory in order for the computations to complete expediently. Therefore, workers have designed a pyramid approach during which MM, SEQM, and DFT methods are used in sequence on an increasingly smaller set of structures (Figure 3).

In the *de novo* ligand design approach, MM is used to sample the gross conformational space of the molecule. High-energy MM conformers are eliminated on steric grounds, which are well represented in MM.[10] Selected low energy MM structures are submitted to SEQM for accurate *geometry prediction*. Although SEQM energies are not always reliable measures of heats of formation, the PM3(tm) level of theory is capable of predicting accurate geometries for organometallic species.[2,11] Consequently, the geometry that results from SEQM optimization is an excellent starting point for the DFT computation. In a benchmark test during this study, the MM-

optimized structure was used as the starting point for the BOP/DNP optimization, which resulted in convergence times up to 7 times slower than when the SEQM-optimized geometry was used as the starting point in the DFT computation.

Both geometric refinement and accurate energy determination in the *de novo* scheme occur with quantum mechanical methods. For organometallic species with a large number of basis functions, DFT is usually the quantum mechanical method of choice.[12]

An open question that has seldom been rigorously addressed in the computational chemistry literature is the analysis of a conformational space once it has been generated. No matter how good a conformational search, if the resulting n -dimensional space is not analyzed correctly, then important conformers may be missed. When comparing experimental, which has an ensemble of conformers, with computational results, the computational portion must contain a good representation of the experimental ensemble. If the computations do not adequately represent the experimental ensemble of conformers, then the comparison is meaningless. In this thesis, the issue of both generation and analysis of conformational space, and the implications to comparing computed to experimental results, will be addressed.

CHAPTER 2. DE NOVO LIGAND DESIGN: UNDERSTANDING STEREOSELECTIVE OLEFIN BINDING TO $[(\eta^5\text{-}C_5H_5)Re(NO)(PPh_3)]^+$ WITH MOLECULAR MECHANICS, SEMIEMPIRICAL QUANTUM MECHANICS, AND DENSITY FUNCTIONAL THEORY

Several important catalytic reactions are thought to be dominated by steric effects. For example, Gladysz has demonstrated that chirally pure, coordinatively unsaturated $[(\eta^5\text{-}C_5H_5)Re(NO)(PPh_3)]^+$ fragments can stereospecifically bind prochiral unsaturated moieties and postulated that the sterically demanding ligands direct the substituents on the unsaturated moiety into the least congested interstice between ligands.[13] To test the hypothesis that steric effects govern the chiral recognition abilities of $[(\eta^5\text{-}C_5H_5)Re(NO)(PPh_3)]^+$, we have used Brown's ligand repulsive energy methodology[14] to determine which isomer of $[(\eta^5\text{-}C_5H_5)Re(\eta^2\text{-unsaturated moiety})(NO)(PPh_3)]^+$ is most *sterically accessible*.[6] Molecular mechanics revealed that the lowest energy isomer with the olefin in the least sterically congested environment is the one that dominates in the experimental reaction.[6] A computationally derived diastereoselective excess, de_{MM}, was able to correctly predict the preferred face of the olefin bound to Re.

Semiempirical quantum mechanics (SEQM) was subsequently used to refine the MM-optimized geometries of $[(\eta^5\text{-}C_5R_5)Re(\eta^2\text{-unsaturated moiety})(NO)(L)]^+$ (R = H, Me; L = PMe_3, PPh_3).[15] Ligand repulsive energies for the olefins in the SEQM-optimized environments were computed and

again revealed that the experimentally observed major isomers were also the favored isomers predicted by SEQM.[15] Finally, the SEQM-based diastereoselective excess, de_{SEQM}, was linearly related to total cone angle of all ligands in $[(\eta^5\text{-}C_5R_5)Re(\eta^2\text{-unsaturated moiety})(NO)(L)]^+$.[15]

In this chapter we report the full *de novo* ligand design model for the recognition of prochiral olefins by $[(\eta^5\text{-}C_5H_5)Re(NO)(PPh_3)]^+$. Specifically, this chapter addresses the problems of: (i) full conformational space sampling of both organometallic fragment and prochiral substrate, (ii) quantification of the steric interaction between fragment and substrate, (iii) appropriate energies computation for each isomer of the substrate bound to the fragment, and (iv) derivation of a meaningful energy-weighted quantitative steric measure for each important isomer. In all cases, the organometallic model consists of $[(\eta^5\text{-}C_5H_5)Re(NO)(PPh_3)]^+$ bound to a series of prochiral α-olefins, CH_2=CHR (R = Me, *n*-Pr, CH_2Ph, Ph, *i*-Pr, *t*-Bu, and $SiMe_3$), for which experimental selectivities are known.[13]

Computational Methods

Molecular mechanics calculations were carried out with Cerius[2] 4.5 available from Accelrys[16] with the Universal Force Field.[17] Semiempirical calculations were carried out with Spartan 5.1 available from Wavefunction,[18] in which the PM3(tm) Hamiltonian was genetics algorithm (GA) optimized for prediction of geometries.[19] Dmol[3] was used for DFT

calculations[20] with the BOP functional,[21] and VPSR relativistic pseudopotential.[22] A double numeric basis set with polarization functions was used for geometry optimization, and double numeric basis set with double polarization functions was used for single point energy calculations. We abbreviate the computation with BOP functional with double numeric basis set with polarization functions as BOP/DNP and double polarization functions as BOP/DNPP. Conformational searches for the olefin, $[(\eta^5\text{-}C_5H_5)Re(NO)(PPh_3)]^+$ fragment, and $[(\eta^5\text{-}C_5H_5)Re(\eta^2\text{-}CH_2{=}CHR)(NO)(PPh_3)]^+$ were performed as reported previously, unless otherwise noted.[6]

Results and Discussion

De Novo Ligand Design

There are four different isomers generated when a prochiral olefin can bind to a $[(\eta^5\text{-}C_5H_5)Re(NO)(PPh_3)]^+$ fragment, **I – IV** in Figure 4. Gladysz has suggested, and we have demonstrated that the *RS*,*SR* isomer contains the olefinic substituents in the least congested environment relative to the ligand set.[6,13] In the study reported here, DFT computations are performed on four isomers (Figure 4) per olefin in order to meaningfully assess the diastereoselectivity of the system. Prior to DFT computation, MM is used to produce 2,000 conformers per isomer **I – IV**,[6] the lowest energy of each isomer is passed onto SEQM[19] for accurate geometry optimization. Finally, these

four structures are then submitted to DFT (BOP/DNP then BOP/DNPP) for accurate energy calculation.

To compare computed results with experiment, the Cambridge Structural Database (CSD) was searched for high-quality (R < 10%), monomeric crystal structures with no reported error and no crystallographic disorder.[23] As anticipated both SEQM and BOP/DNP structures agree well with structural parameters obtained from the CSD (Table 1). As the computational method becomes more sophisticated (MM to SEQM to DFT), the olefin becomes more orthogonal to the Re-centroid vector, as evidenced in the Re-C(olefin) bond distances (Table 1; 0.02 Å difference in the crystal structures,[23] 0.28 Å difference by MM, 0.02 Å difference by PM3(tm), and 0.08 Å by BOP/DNP). The Re-nitrosyl interaction (Re-N distance and Re-N-O angles) is modeled well with BOP/DNP but less so with PM3(tm). Conversely, the Re-Cp is better modeled with PM3(tm) than BOP/DNP (Table 1). Finally, the olefinic C=C bond eclipses the Re-P bond vector (Re-C(olefin centroid)-C_{ipso}-P torsion angles of –175(2)/+9(5)° by PM3(tm) and –172(4)/9(5)° by BOP/DNP). This eclipsing of the olefinic C=C bond with the Re-P bond vector is thought to optimize the overlap between filled Re *d*-orbitals and olefinic π*-orbitals.[13] The negative torsion angles result from rotomers **I** and **III** in Figure 4.

Steric Size of the Olefin in the $[(\eta^5\text{-}C_5H_5)Re(NO)(PPh_3)]^+$ Environment Computed from SEQM and DFT Structures

Brown defined a new measure of steric size in the 1990's by making use of MM. The Ligand Repulsive Energy, E_R, is defined as the amount of Van der Waals repulsion between a ligand and the environment around that ligand. Working with the prototypical $Cu(CO)_5$ environment, Brown defined

$$E_R = -r_e\left(\frac{\partial E_{vdW}{}^{Rep}}{\partial r}\right) \qquad (1)$$

Where r_e is the equilibrium Cu-donor atom distance, $E_{vdw}{}^{Rep}$ is the van der Waals repulsive energy and r is the variable Cu-donor atom distance. Brown and White have extended the calculation of ligand repulsive energies to a wide variety of substituents (amines, sulfides, olefins, organics, etc.). When a moiety other than $Cu(CO)_5$ is used, the label of ligand repulsive energies is E'_R (fragment).

Literature results have suggested that any good representation of the structure of an organometallic complex is an acceptable starting point for a ligand repulsive energy calculation.[7-9] It has been shown that the *trend in ligand repulsive energy* does not depend significantly on the prototypical fragment used for the calculation.[7-9,24-26] It has also been shown that ligand repulsive energies do not depend greatly on the force field employed for their computation.[9] In this chapter, we now address the question of whether ligand repulsive energies determined from MM, SEQM, or DFT-optimized

structures are comparable. Ligand repulsive energies were computed with ERCODE.[9]

Plots of ligand repulsive energy from MM or SEQM structure against ligand repulsive energy from the DFT structure are linear and almost parallel with a 20 kcal/mol difference in intercepts (Figure 5). The small amount of scatter in the plots is mostly likely due to conformational effects (see below). We may conclude that the ligand repulsive energy methodology provides a robust, quantitative measure of steric effects invariant to prototypical fragment, MM force field, or level of theory used to derive the starting structure.

DFT Model of Stereoselective Binding of Prochiral α-Olefins to $[(\eta^5\text{-}C_5H_5)Re(NO)(PPh_3)]^+$

All the lowest energy conformers generated from the SEQM study[15] were submitted to Dmol[3] for geometry optimization with the BOP functional with a double numeric basis set with polarization functions (BOP/DNP) and the VPSR relativistic pseudopotential.[20-22] Single point energies were computed for the BOP/DNP optimized structures with a double numeric basis set with double polarization functions (BOP/DNPP). The BOP/DNP-optimized structures were submitted to ERCODE for ligand repulsive energy computation. The DFT and ERCODE results are summarized in Table 2.

To ensure the BOP functional[21] provides consistent results, single point energy calculations with DNPP basis set were performed on all isomers of $[(\eta^5\text{-}C_5H_5)Re(\eta^2\text{-}CH_2{=}CHR)(NO)(PPh_3)]^+$, R = Me, *i*-Pr and Bn (Figure 4), with the BLYP[27,28] and BP[27,29] functionals in Dmol[3].[20] In addition, single point energies were computed for the $[(\eta^5\text{-}C_5H_5)Re(\eta^2\text{-}CH_2{=}CHMe)(NO)(PPh_3)]^+$ complex with the B3LYP[28,30] functional in Gaussian 98.[31] Energies relative to the lowest energy isomer for a given olefin are tabulated in Table 2. There is good agreement between the relative energies of the isomers across the functionals studied. In all cases, the *RS,SR* isomers have the lowest BOP/DNPP energies, in agreement with Gladysz's hypothesis and our previous results.[6,13,15]

Single point BOP/DNPP energies for the BOP/DNP-optimized structures are shown in Table 3. These energies are reported relative to the lowest energy structure for each olefin. As anticipated, the *RS,SR* isomers all have the lowest energies.[6,13,15] With the exception of the 1-butene ligand, the energies of the isomers increase as *RS,SR* < *RR,SS* < *RS,SR*2 < *RR,SS*2 (Table 2).[6,13,15] This energy trend is expected based on the simple rationalization that the energy of an isomer increases as the substituent on the α-olefin interacts with the sterically demanding ligands on Re.[6,13,15] The olefinic substituent in the 1-butene ligand is responsible for the break in energy trend, which is an indication of a potential problem in the conformational search strategy employed.

Computational Measure of Diastereoselectivity, *de*, and Conformational Searching

In order for a complex to efficiently participate in the stereoselective binding of a prochiral olefin, two conditions must be satisfied: (i) one isomer must have a lower energy than the others, and (ii) one isomer must contain the olefin in a less sterically congested environment than the others. Condition (i) is met when an isomer has a low BOP/DNPP energy whereas condition (ii) is met when one isomer has a low E''_{R} (E''_{R} is the ligand repulsive energy computed with the title complex from a BOP/DNP-optimized geometry).

In the literature on this series, MM and SEQM results were reported that enabled us to rationalize prochiral olefin binding using a purely steric model.[6,15] These results assumed that only one conformer per isomer dominated in the recognition of the prochiral olefin (Figure 4). However, diastereoselectivities (see below) computed on olefins with conformationally flexible substituents did not agree with experiment. This prompted the question of whether certain important conformers were missing from consideration.

Combined QM/MM methods assume that the reaction center of a molecule can be treated with quantum mechanics while the conformationally flexible, "steric", portions can be treated with molecular mechanics affording

meaningful results in a modest amount of time.[32] Therefore, to locate any missing minima, we undertook a modified MM/DFT approach.

Each BOP/DNP optimized isomer was imported from Dmol[3] into Cerius[2] and all atom positions frozen except those atoms in the substituent on the olefin. The conformational space of the substituent on the olefin was explored by means of a grid search and each resulting conformer was partially energy minimized with the UFF (only the atoms in the substituents were allowed to geometry optimize).[17] The torsion angle window was set to –90° to +90° for substituents with a C_2 axis and –180° to +180° for substituents with a C_3 axis. The grid was set to 1° or 10°, depending on the total number of conformers generated (for example, a 1° grid was used for structures with only one rotatable bond whereas 10° grid was used for the $[(\eta^5\text{-}C_5H_5)Re\{\eta^2\text{-}CH_2{=}CH(n\text{-}Pr)\}(NO)(PPh_3)]^+$ isomers). The results for the grid search on the *RS,SR*2 isomer for $[(\eta^5\text{-}C_5H_5)Re\{\eta^2\text{-}CH_2{=}CH(n\text{-}Pr)\}(NO)(PPh_3)]^+$ are shown in Figure 6. (The isomer labels in Figure 4 are shown in Table 4.) There are several redundant minima in Figure 6; for example, the data point at A: (180°, 180°) is the same as (A): (–180°, –180°), (A): (–180°, 180°), etc. These redundancies are indicated by placing the isomer label in parentheses. The minimum at approximately (180°, –60°) was found to converge to A after full BOP/DNP geometry optimization.

All potential minima from the grid search for $[(\eta^5\text{-}C_5H_5)Re(\eta^2\text{-}CH_2{=}CHBn)(NO)(PPh_3)]^+$ were submitted to Spartan and the structures

geometry optimized under the same restraint as the MM-structures (i.e., the BOP/DNP-optimized portion of the molecule was frozen). After SEQM optimization, many of the MM minima were found to be redundant. For example, the MM grid search found four minima for the *RS,SR* isomer, whereas SEQM only located two, one of which was not the global minimum found in the MM search. Although there is no guarantee that the lowest energy structure predicted with molecular mechanics is the same as the lowest energy structure predicted by SEQM, we were perturbed by the reduction of four MM minima to two SEQM minima. Furthermore, 16 of the 28 MM minima for the $[(\eta^5\text{-}C_5H_5)Re\{\eta^2\text{-}CH_2{=}CH(i\text{-}Pr)\}(NO)(PPh_3)]^+$ isomers did not converge in SEQM. Therefore, the SEQM step was skipped and the partially optimized MM structures were imported directly into Dmol[3] for full geometry optimization at the BOP/DNP level (Table 4; Figure 6).

Consider the **B** and **C** conformers of the *RS,SR* isomer for the benzyl substituent: the BOP/DNP energies are very similar, as are the torsion angles predicted by MM and determined by DFT. (Since there is a C_2 axis of symmetry about the phenyl ring of the benzyl substituent, a torsion angle of 65.4° is equivalent to 114.6°.) With Chem 3D Pro, these two structures were found to be superimposed with less than 0.1 RMS error and 0.01 RMS gradient. Therefore, we take these two conformers to be the same and conclude that the MM-predicted conformer with a $C_{ipso}\text{-}CH_2\text{-}C_{ipso(Ph)}\text{-}C_{ortho}$ torsion angle of 64.4° is not an energy minimum according to the more

sophisticated DFT level of theory. Similar analysis shows that conformers **A** and **B** of the *RS,SR*2 isomer for the *n*-Pr substituent are identical (Figure 7 and Figure 8). All redundant conformers, defined by less than 0.1 RMS error and 0.01 RMS gradient in Chem 3D Pro, close torsion angles and close energies, are italicized in Table 4 and are not considered in any of the following analyses.

By restraining the BOP/DNP-optimized atomic positions in the immediate vicinity of the metal center in the MM grid search, we mimic the ONIOM methodology. [33,34] However, re-optimization of the entire structure with BOP/DNP results in the finding that certain MM-predicted minima do not exist. If these minima are included in the computation of an energy-weighted property, then an incorrect result is highly likely. Therefore, an ONIOM type methodology is not appropriate for the system under investigation and the combined MM-SEQM-DFT-MM-DFT approach, illustrated in Figure 9, yields more accurate results.

It follows from our results that the initial MM conformational search is not as critical as we originally predicted and significantly fewer structures are acceptable. The first SEQM step is still required in order to decrease the amount of computer time necessary for the convergence of the DFT jobs. The most critical part of the conformational search is the freezing of conformationally inflexible portions of the molecule in the DFT-optimized structure followed by a grid search performed on the olefinic substituent.

The final set of hybrid DFT/MM minima requires full optimization by means of DFT methods since MM is not sufficiently reliable to predict the final structure or energy of the system. If we are only interested in the lowest energy structure, then the original MM-SEQM-DFT approach is sufficient; however, if we need to identify *all minima* (see below) that can participate in a reaction, then the original MM-SEQM-DFT approach is not sufficient.

Recomputed Diastereoselective Excess, de_{DFT}

In the literature, we have introduced a computationally derived diastereoselective excess, de_{MM} and de_{SEQM}.[6,15] If ΔE_i is the relative BOP/DNPP energy of conformer i and $kT = 0.592476141388$ kcal/mol at 298.15 K, then the Boltzmann weight of conformer i, w_i, is

$$w_i = \frac{\exp\left(-\frac{\Delta E_i}{kT}\right)}{\sum \exp\left(-\frac{\Delta E_i}{kT}\right)} \tag{2}$$

We define the Boltzmann weighted ligand repulsive energy computed from the BOP/DNP optimized isomer for conformer i, $\langle E''_{\mathrm{R}}\rangle_i$, as

$$\langle E''_{\mathrm{R}}\rangle_i = w_i \times \exp\left(-\frac{\Delta E''_{\mathrm{R}}}{kT}\right) \tag{3}$$

where $\Delta E''_{\mathrm{R}}$ is the relative ligand repulsive energy for isomer i. Finally, if $\langle E_{RS,SR}\rangle$ is the Boltzmann weighted ligand repulsive energy for the RS,SR isomer as defined in equation (3), $\langle E_{RS,SR2}\rangle$ is the same quantity for the

*RS,SR*2 isomer, etc., then the computed diastereoselective excess, de_{DFT}, is given by

$$de_{DFT} = \left(\langle E_{RS,SR}\rangle + \langle E_{RS,SR2}\rangle\right) - \left(\langle E_{RR,SS}\rangle + \langle E_{RR,SS2}\rangle\right) \quad (4)$$

Having identified the missing conformers with the combined MM-SEQM-DFT-MM approach, illustrated in Figure 9, it is possible that an MM-based de_{MM} will now compare more favorably with experimental *de* than reported earlier.[6] Unfortunately, the de_{MM} values are not in good agreement with experiment even when the additional conformers are considered; Table 5. The internal energy differences between diastereomers that exhibit a *de* = 0.90 is small (1.7 kcal/mol at 298.15 K) and molecular mechanics energies computed with the UFF are not sufficiently accurate to quantitatively predict experimental *de*. Therefore, we must turn to the more accurate BOP/DNPP energies in order to obtain a computed diastereoselectivity that can be meaningfully compared to experiment.

With the exception of the *t*-Bu and $SiMe_3$ substituents, there is good agreement between de_{DFT} and experimental *de* (equation (4); Table 6). However, if we omit the additional conformers found after the MM grid search, then the agreement between computed and experimental *de* is poor. For example, de_{DFT} for the Bn substituent increases from 0.806 with all conformers considered (Table 3) to 0.989 with only the lowest energy conformer for each of the four isomers (Table 4). The agreement between computed (0.801) and experimental *de* (0.88) for the benzyl substituent is

particularly remarkable as Bn is often an outlier in comparisons between computed and experimental physical properties.[6,15]

The high computed de_{DFT} values for the *t*-Bu and $SiMe_3$ substituents are a consequence of the *RS,SR* isomers having a low BOP/DNPP energy and a low E''_R value. For both of these substituents, the high energy, high E''_R structures contain the substituent on the olefin displaced significantly from the C=C plane. For example, the average Re-C(*t*-Bu) distance is 3.64 Å for the high energy isomers and 3.46 Å for the *RS,SR* isomer. Similarly, the average Re-Si distance is 3.94 Å for the high energy isomers and 3.73 Å for the *RS,SR* isomer. Both the energies and the E''_R values for three of the four isomers are sufficiently large to force the Boltzmann weights to zero. Consequently, the diastereoselectivity is effectively based on a single conformer for the *t*-Bu and $SiMe_3$ substituents whereas all other structures contain more than one competent conformer.

Ligand repulsive energies only consider the steric interaction between olefin and $[(\eta^5\text{-}C_5H_5)Re(NO)(PPh_3)]^+$ fragment. It is possible that there is an electronic effect that comes into play for the *t*-Bu and $SiMe_3$ substituents that accounts for the low experimental *de* values.

Conclusions

A rigorous DFT approach to the stereoselective binding of prochiral α-olefins to $[(\eta^5\text{-}C_5H_5)Re(NO)(PPh_3)]^+$ has been undertaken. A new

conformational search strategy has been developed that successively uses MM-SEQM-DFT-MM-DFT in order to locate all minima that can participate in a reaction. With all conformers identified, a computed diastereoselective excess, de_{DFT}, shows acceptable agreement with experiment for all olefins except the sterically bulky, electron rich CH_2=CH(*t*-Bu) and CH_2=CH($SiMe_3$) olefins.

CHAPTER 3. GRAPH THEORETICAL ANALYSIS OF THE CONFORMATIONAL SPACE IN CYCLOPENTADIENYL COMPLEXES OF RHENIUM: IMPLICATIONS TO PREDICTIONS OF DIASTEREOSELECTIVITY

In Chapter 2 we recognized that using only one conformation per olefin orientation (Figure 4) gave rise to erroneous results when the olefin contains many conformational degrees of freedom. It was also recognized that stereoselectivity could be computationally modeled using a combination of MM-SEQM-DFT-MM-DFT (Figure 9). However, in Chapter 2, the conformational space derived from the second MM step (Figure 6) was analyzed by inspection rather than using a rigorous approach. Fortunately, the olefins used in the experimental study, which were considered in the computational study presented in Chapter 2, all contained two or fewer rotatable bonds. Thus, the plot of torsion angles against energy shown in Figure 6 represents a three-dimensional surface. For molecules with n rotatable bonds, an $(n + 1)$ torsional hypersurface must be analyzed, which is impossible to achieve by visual inspection. Therefore, a rigorous mathematical approach to the analysis of torsional hypersurfaces must be developed, which is the central theme to Chapters 3 and 4.

Each set of minima as represented in Figure 6 represents a cluster of chemical structures that are energetically and structurally similar. Rigorous mathematical analysis of these clusters will ensure that we locate all

structural and energetic minima for the conformational space of a given molecule.

Graph Theoretical Approach to Cluster Analysis

Given a similarity measure, cluster analysis seeks to partition a data set into subsets containing members that are more similar to themselves than to any members of other subsets comprising the partition. The primary interest of this paper is to identify natural groupings of conformers based on their torsion angles alone. In such a setting, the conformers in these natural groupings are close to each other with respect to the Euclidean metric. We thus use the Euclidean metric as our similarity measure.

We have observed that in many instances, a set of partially optimized structures for a chemical ensemble has natural groupings with differing densities. In other words, the number of partially optimized structures in a natural grouping within the data set may vary with respect to the volume occupied by the grouping in the torsional space. Thus, it is important to find a method of computationally identifying these natural groupings, which does not depend on global distance parameters.

Our solution to this problem is to represent the data set as an undirected similarity graph with edges weighted by distance. In the similarity graph setting, we may impose discrete clustering parameters that do not depend on global properties of the similarity graph. This approach

addresses weaknesses inherent in published clustering methodologies in the chemical literature in that it does not assume the shape of clusters to be spherical and it does not assume homogeneous density of clusters.[69]

Existing Cluster Analysis Methodologies

Cluster analysis techniques comprise two categories: hierarchical and non-hierarchical methods. Hierarchical methods identify clusters via a recursive process that preserves existing clusters at any step of the method as subclusters of clusters in following steps, while non-hierarchical methods are not guaranteed to have this property.

We may consider Shenkin-McDonald's method and the k-means method as illustrative examples. The Shenkin-McDonald method is hierarchical, while k-means is non-hierarchical.

Although the non-hierarchical k-means method is relatively fast computationally as compared to the Shenkin-McDonald method since k-means does not require computation of all pairwise distances between members of the data set, k-means must be supplied with the number of clusters as a starting parameter. This is a disadvantage when the natural number of clusters existing in a data set is unknown. Further, k-means tends to identify spherical clusters while many data sets have non-spherical natural clusters.

The hierarchical Shenkin-McDonald method has the advantages of not requiring a starting number of clusters to be given as a parameter and of being able to identify non-spherical clusters at the computational expense of computing all pairwise distances, but suffers from its single-linkage nature, which tends to produce chained clusters.[69]

The method reported in this paper seeks to rectify the single-linkage problem by requiring identified clusters to have high discrete density (our definition of discrete density is a simple one; more complicated notions have been introduced by Hartuv-Shamir, Matula, and others). We propose our method as a clustering methodology that is more readily able to identify natural clusters in non-homogeneous data, without assumptions on the shapes of these clusters.

cClus-A Implementation

The cClus-A© algorithm is a graph-theoretic approach for identifying clusters. It has two independent components controlling first the construction of a similarity graph for the data being analyzed and then the isolation of locally dense regions in the data.

Construction of Similarity Graph

The vertices of the similarity graph are defined to be the conformers of the data being analyzed and edges between vertices are weighted by distance between conformers, distance being determined by the Euclidean metric on the space of torsion parameters. Conformer energy is not a component of this distance measure.

The torsion angles from a conformational search are read in from a tab-delimited input file and stored in the two-dimensional array ConformerData[ ][ ] so that ConformerData[0] is the array of torsion parameters associated with the first conformer. A two-dimensional array DistanceMatrix[ ][ ] is then initialized, and for each pair (i,j) of conformers, the Euclidean distance between ConformerData[i] and ConformerData[j] is computed and stored in DistanceMatrix[i][j]. Construction of the distance matrix is the most computationally expensive part of the algorithm.

The DistanceMatrix represents the adjacency matrix for the complete similarity graph with edges weighted by distance. By selectively setting entries of the distance matrix to 0, we effectively remove edges in the graph. We sparsify DistanceMatrix[ ][ ] by considering each column in turn, setting all but the n smallest distances in each column to 0. The resulting matrix is no longer guaranteed to be symmetric, a necessary condition for the second part of the algorithm, so a symmetrization loop is used to set DistanceMatrix[j][i] equal to DistanceMatrix[i][j] for all (i,j) with j taking on values from 0 to the number of conformers and i taking on values from j to

the number conformers. At this point, DistanceMatrix[ ][ ] is the adjacency matrix for an edge-weighted, undirected similarity graph representing locally compact regions of the conformation data.

Isolation of Dense Connected Components

We define the density of a connected component to be the number of edges in the component divided by the number of vertices. Denoting the number of vertices of a component by n, we note that the density of the component must be in the interval from (n-1)/n to (n-1)/2. A high-density connected component is defined to be any component density greater than (2n-2)/(n+2).

The connected components of the similarity graph are determined more efficiently by changing the representation of the similarity graph to a sparse data structure conformerDistMap[ ][ ] so that conformerDistMap[*i*][*j*] has value DistanceMatrix[*i*][*j*] whenever DistanceMatrix[*i*][*j*] is nonzero. The procedure shortestDistance accepts conformerDistMap[ ][ ] and a conformer number start as parameters and returns a list of distances from start to each conformer in the connected component of start. For each call of shortestDistance, the conformers in the connected component of start are all assigned the same cluster number. The procedure shortestDistance is called recursively until all conformers are assigned a cluster number. The

minimum-energy conformer of each high-density connected component is then given as output.

Results and Discussion

Comparison of Clusters Generated by Different Methods

The conformational space of $[(\eta^5\text{-}C_5H_5)Re(\eta^2\text{-olefin})(NO)(PPh_3)]^+$ was derived as follows (Chapter 2). The structure was built in Cerius[2] and subjected to UFF-energy minimization. A thorough conformational search was performed, as described in Chapter 2 and in the literature.[6,15,35] The lowest energy structure for each isomer (Figure 4) was imported into Spartan and PM3(tm) geometry optimized.[15] The PM3(tm) optimized structures were then BOP/DNP optimized in Dmol[3]. In this chapter we concentrate on two complexes: $[(\eta^5\text{-}C_5H_5)Re(\eta^2\text{-}CH_2CHBn)(NO)(PPh_3)]^+$ and $[(\eta^5\text{-}C_5H_5)Re(\eta^2\text{-1-butene})(NO)(PPh_3)]^+$ since they both have two rotatable bonds in the olefinic substituent. All others complexes have one or no rotatable bonds in the olefinic substituent, so the analysis of the conformational space is trivial. All atoms were then frozen except those involved in the olefinic substituent, which were systematically varied to generate a torsional grid such as the one illustrated in Figures 6 and Figure 10.

It is possible that the non-hierarchical k-means clustering algorithm found in the commercial program SAS could adequately analyze the conformational space of $[(\eta^5\text{-}C_5H_5)Re(\eta^2\text{-}CH_2CHBn)(NO)(PPh_3)]^+$ and $[(\eta^5\text{-}$

C_5H_5)Re(η^2-1-butene)(NO)(PPh_3)]$^+$ even though k-means assumes spherical clusters and the number of clusters has to be supplied by the user. Within SAS, a cubic clustering criterion plot can be constructed, which typically shows a discontinuity at the ideal number of clusters. When SAS was supplied with raw data, the clustering algorithm failed and was not able to reproduce the number of structures that were determined in Chapter 2 (Table 7). Therefore, the data were conditioned to remove all structures that were higher than about 3 kcal/mol from the lowest energy structure in the set. The conditioned data for the *RR,SS* isomer of [(η^5-C_5H_5)Re(η^2-1-butene)(NO)(PPh_3)]$^+$ is shown in Figure 11. Notice that the clusters illustrated in Figure 11 closely mirror those considered in Figure 6.

The k-means clustering algorithm in SAS assumes a spherical cluster, which can result in conformers that are missed and also results in conformers that are considered more than once. Therefore, we turn our attention to using a graph theoretical analysis of the conformational space, contained in a new program created; cClus-A.

When the data set illustrated in Figure 11 was analyzed with cClus-A described above, ambiguous results were found as with the SAS k-means approach; Table 8. In this example, the two automated approaches yield different results, in that SAS misses one distinct isomer, whereas cClus-A identifies all low energy conformations. Across all isomers of [(η^5-C_5H_5)Re(η^2-1-butene)(NO)(PPh_3)]$^+$, SAS misses a total of three unique conformers

whereas the graph theory code only misses one. Therefore, the k-means clustering methodology in SAS will not be used any further in this thesis. cClus-A will be further tested with $[(\eta^5\text{-}C_5R_5)Re(\eta^2\text{-olefin})(NO)(PMe_3)]^+$, R = H and Me, described below and more complicated torsion angle hypersurfaces, presented in Chapter 4.

In an effort to confirm that increased steric congestion about the metal center results in increased stereoselectivity towards a prochiral olefin, the complexes $[(\eta^5\text{-}C_5R_5)Re(\eta^2\text{-olefin})(NO)(PMe_3)]^+$, R = H and Me, were modeled by means of the *de novo* design strategy summarized in Figure 9.[15] The conformational spaces for $[(\eta^5\text{-}C_5R_5)Re(\eta^2\text{-olefin})(NO)(PMe_3)]^+$ were sampled in the same manner as for $[(\eta^5\text{-}C_5H_5)Re(\eta^2\text{-olefin})(NO)(PPh_3)]^+$ (Chapter 2). A graph theoretical analysis was performed of the torsional space generated from the partially-UFF optimized grid search described in Chapter 2 and the results are summarized in Table 9.

Application of cClus-A to Organometallic Systems

Work in this thesis has focused on the generation and analysis of the conformational space of $[(\eta^5\text{-}C_5R_5)Re(\eta^2\text{-olefin})(NO)(L)]^+$ (R = H, Me, and L = PPh_3, and PMe_3) complexes.[6,15,35] Since the complexes are chiral with a stereogenic center at Re and the *ipso* carbon atom of the olefin, there are four possible stereoisomers that results when the prochiral olefin binds to the $[(\eta^5\text{-}C_5R_5)Re(NO)(L)]^+$ fragment, illustrated in Figure 4. The conformational

space of each of the isomers of $[(\eta^5\text{-}C_5R_5)Re(\eta^2\text{-olefin})(NO)(L)]^+$ was derived as follows. The structure was built in Cerius[2] and subjected to UFF-energy minimization. A thorough conformational search was performed, as described in the chapter 2.[6,15,35] The lowest energy structure for each isomer was imported into Spartan and PM3(tm) geometry optimized.[15] The PM3(tm) optimized structures were then BOP/DNP optimized in Dmol[3]. For complexes that contain an olefinic substituent with one or more rotatable bond, a second conformational grid search was employed, as described in Chapter 2.

For illustrative purposes, we focus on $[(\eta^5\text{-}C_5H_5)Re(\eta^2\text{-}CH_2CHBn)(NO)(PPh_3)]^+$ since the complex has two rotatable bonds in the olefinic substituent. Prior to applying cClus-A to the analysis of the torsional space of these two complexes, the data set must be conditioned to remove extraneous high energy conformers and yield a data set with discrete clusters. Since a conformer that is greater than 3 kcal/mol higher in energy than the lowest energy conformer has negligible Boltzmann weight, we set 3 kcal/mol as the energy cutoff to condition the data. The conditioned data for the *RR,SS* isomer of $[(\eta^5\text{-}C_5H_5)Re(\eta^2\text{-}CH_2CHBn)(NO)(PPh_3)]^+$ is illustrated in Figure 12.

The conditioned data were submitted to cClus-A for cluster analysis. Figure 12 shows the conditioned raw data alone with the structures that cClus-A determines as unique.

To test the robustness of cClus-A, the torsion angles spaces of a variety of complexes were considered: $[(\eta^5\text{-}C_5H_5)Re(\eta^2\text{-1-butene})(NO)(PPh_3)]^+$, $[(\eta^5\text{-}C_5H_5)Re(\eta^2\text{-olefin})(NO)(PMe_3)]^+$, and $[(\eta^5\text{-}C_5Me_5)Re(\eta^2\text{-olefin})(NO)(PMe_3)]^+$. Conformational searches on these systems were performed as described above and in the literature (Figure 6).[6,15,35] In all cases, cClus-A was able to unambiguously locate all discrete clusters in the data sets.

CHAPTER 4. CONFORMATIONAL SPACE OF CHIRAL DIPHOSPHINE RHODIUM(I) CATALYST PRECURSORS

Organometallic complexes are currently being widely used to carry out difficult transformations in the synthesis of organic molecules with diverse physical properties.[36] In particular, the roles of chiral metal complexes in synthesis and catalysis are of great current interest. For example, bidentate phosphine Rh(I) complexes serve as catalysts for asymmetric hydrogenation;[37-41] chiral Re(I) centers selectively complex prochiral substrates to form complexes that can serve as templates for subsequent reactions;[13,42,43] osmium oxide catalysts enable enantioselective dihydroxylations;[44-46] and chiral Mn complexes are catalysts for asymmetric oxidations.[47-50] In such systems, the enantioselectivity is based to a large extent on differential *steric* effects in a diastereomeric pre-equilibrium or transition state, even though steric effects may be mediated in some cases by electronic factors.[51,52] Molecular modeling affords a means to a deeper understanding of the steric factors at work in diastereoeselectivity. Further, such understanding can lead to a cost-effective and timesaving capacity for the design of new systems. With the advent of faster computers, the application of molecular modeling methods to inorganic complexes is increasing.[53-55] In particular, Landis has recently modeled rhodium catalyzed asymmetric hydrogenation using DFT methods.[56,57]

An effective molecular model of diastereoselectivity must provide a realistic comparative model of the transition states and, if applicable, any diastereomeric pre-equilibrium for the reaction. The model must also take account of the possibility of multiple kinetically competent conformers of the ground state catalyst and reactant, and of the transition states generated from them. Chiral selectivity in HPLC and related chiral separations[58,59] and enantioselective interactions[60] have some of the properties of the systems of interest here. Binding of an analyte to a chiral stationary phase (CSP) has been modeled using both molecular mechanics and molecular orbital methods.[58,59] An important characteristic of these systems is that equilibria between several conformers of the analyte-CSP complex lie within a narrow energy range of the lowest energy form. The hydrogen-bonding equilibria involving a series of polyamides with varying conformational preferences represent yet another example in which it is necessary to model a Gibbs ensemble of molecules.[61]

This chapter describes the application of rigorous conformational analysis to understand the ensemble of conformers available for reaction in asymmetric hydrogenation Rh(I) catalysts. A large number of chiral bidentate ligands has been synthesized and studied because of their potential as ligands in hydrogenation catalysis (Figure 10).[37-41,62] In this chapter, we use molecular mechanics to model $[Rh(P\text{-}P^*)(nbd)]^+$, where P-P* represents a chiral bidentate phosphine ligand, nbd = norbornadiene, which has allowed

us to established a methodology for identifying the important conformational minima in a flexible system. The approach used in this chapter to analyze the conformational spaces is the same as the one used in Chapter 3. In addition, bidentate phosphines used in asymmetric hydrogenation have four torsion angles about the Rh reaction center. Therefore, we have a more rigorous test of cClus-A.

Results and Discussion

Determination of the Conformational Minima in $[Rh(P\text{-}P^*)(nbd)]^+$ Complexes Without cClus-A

The molecules are represented by an extended MM2 type force field model, with parameters as described elsewhere and in the Methods section.[7,14,24-26,63-66] The torsional degrees of freedom can be labeled according to whether the aryl group involved is above or below the coordination plane comprised roughly of Rh, the two P atoms and centroids of the bound olefins, Figure 11. The P atom to the left in Figure 11 is labeled a, that on the right is b. The ϕ/ψ torsion angle convention used is as follows: torsion angles of 0° have the aryl with a substituent in the *ortho* position aligned parallel to the Rh-P bond axis, and with the substituent pointing towards the Rh atom. When the substituents in the *ortho* positions are identical (commonly H), the torsional angles are modulo 180°.

The edge/face torsional degrees of freedom of importance in this study are labeled ϕ_a and ϕ_b for the "up" torsions, and ψ_a and ψ_b for the "down" torsions. As illustrated in Figure 11, which corresponds to the ligand backbone in the λ configuration, the ϕ_a phenyl group is roughly axial with respect to the coordination plane, whereas the ϕ_b phenyl group is roughly equatorial. Correspondingly, the ψ_a phenyl group is roughly equatorial and the ψ_b phenyl group is roughly axial. The torsion angles that define these positions of the phenyl groups, often called elevation angles, are of the form P-Rh-P-C_{phenyl}. The two torsions for phenyl groups above the plane are labeled α_a and α_b, those for phenyl groups below the plane are labeled β_a and β_b. As Landis and coworkers have pointed out, the distinction between *pseudo*-axial and *pseudo*-equatorial orientations varies from ligand to ligand, depending on the puckering in the ligand backbone, among other factors.[66]

The computations will be illustrated using the *S,S*-chiraphos complex, in which the coordinated diphosphine is in the δ configuration (Figure 11).[38] An unconstrained Monte Carlo search of the four phenyl ring ϕ and ψ torsional degrees of freedom (all others are determined by the conformation of the chelate ring) is carried out as follows: 2,000 structures are produced by allowing each torsion angle to vary between -180° and +180°.[67] (As discussed below, the α/β torsions are determined by the ligand backbone conformation chosen, or are dependent on the values of the ϕ and ψ angles.) All four phenyl torsion angles (ϕ, ψ) are varied simultaneously and by randomly different

amounts. Then the structure is partially minimized (conjugate gradient minimizer, 5,000 steps of minimization with a termination criterion of 0.1 kcal mol^{-1} $Å^{-1}$). Two-dimensional plots of torsion angles result; examples are shown in Figure 12 and Figure 13. Those conformers within 10 kcal mol^{-1} of the global minimum are shown in blue and the rest in pink. It is immediately clear from Figure 12 and Figure 13: (a) there is nearly perfect redundancy modulo 180° in both dimensions; (b) nearly all the energy-minimized structures fall within a narrow range of values of ϕ_a and ψ_b; the range of values of ϕ_b and ψ_a is larger, but in these cases as well there are "forbidden" values of the torsion angle. When all 2,000 partially minimized structures are re-minimized using a Fletcher-Powell minimizer to discard saddle points, the range of observed torsion angles shrinks to a tightly bound cluster in all dimensions (Figure 14).

The graphs in Figure 14 identify all allowed values of ϕ_a, ϕ_b, ψ_a, and ψ_b. However, all possible *combinations* of these angles are not structurally allowed. To find the allowed combinations of torsion angles, a series of 2D plots of P-aryl torsion angles was generated: (ϕ_a vs. ϕ_b), (ϕ_a vs. ψ_a), (ϕ_a vs. ψ_b), (ϕ_b vs. ψ_a), (ϕ_b vs. ψ_b), and (ψ_a vs. ψ_b). The torsional angles characteristic of the clustered minima in each two-dimensional plot were tabulated. By systematic examination of the 2D data it is possible to identify and eliminate those combinations of torsional angles forbidden by structural constraints. For example, for chiraphos the ϕ_a vs. ϕ_b plot (Figure 14) allows a minimum at

ϕ_a = -90° and ϕ_b = -90° without specifying ψ values. It is possible, therefore, that a minimum exists with ϕ_a = -90°, ϕ_b = -90°, ψ_a = -90°, and ψ_b = -90°. When we examine the ϕ_a vs. ψ_a plot, however, we find no minimum at ϕ_a = -90°, ψ_a = -90°. By correlating all 2D plots, it becomes evident that only four structurally allowed combinations of torsion angles exist for the chiraphos complex within 10 kcal mol^{-1} of the lowest energy form. This set of four structures forms the basis for further determination of the conformational minima.

The lowest energy structure in the original ensemble of 2,000 conformers was selected and the phenyl ϕ and ψ torsion angles changed successively to match the values for the four structures determined as described above. Each structure so obtained was subjected to full energy-minimization using a Fletcher-Powell minimization routine (termination criterion 0.01 kcal mol^{-1} $Å^{-1}$), then further subjected to 3.6 ps of molecular dynamics at 500 - 600 K, followed by Fletcher-Powell minimization to ensure a refined minimum energy structure. The energy and four torsion angles, ϕ_a, ϕ_b, ψ_a and ψ_b, for each refined structure were extracted to ensure each structure was unique. (In some cases, for ligands other than chiraphos, following molecular dynamics two adjacent minima on the torsion angle hypersurface were found to converge on a single set of torsion angles and energy, presumably because the barrier to their interconversion is small. Therefore, in some cases there were fewer refined minimum energy

structures than crude minima. In such cases the original torsion angle plots were examined to ensure that all final minima were structurally feasible.)

Table 10 lists the conformer energies and values of the torsion angles, ϕ/α or ψ/β, for each P-phenyl ring. The adequacy of the overall approach is established in part by criteria of stability and convergence: (a) The average potential energy of the 2,000 fully minimized conformers is independent of the sample size in cases where this has been varied from 2,000 to 4,000 to 8,000. The second moment of energy, the standard deviation, is also largely independent of sample size. (b) The minimization procedure leads to the same small number of major minimized structures regardless of where the unconstrained Monte Carlo procedure sets the initial structure. (c) The symmetry of the molecular system, present as a two-fold symmetry of the phenyl group torsions, is reflected in the distributions of energy-minimized structures.

Table 10 shows that up to four conformational minima lie within the 10 kcal mol^{-1} range of the global energy minimum. In comparing the torsional angles characteristic of these structures we find that the lowest energy forms do not necessarily have torsional angles that closely match those observed in crystal structures of diene complexes involving these same ligands.[68] In any event, whether there is an energy-minimized structure with torsional angles characteristic of those observed in the solid state, it is clear also that other structures of comparable energy exist, in agreement with the

conclusions of Giovanetti *et al*. on the basis of their approach to exploring the conformational energy surface in such systems.[66]

The results of the modeling indicate that for the more rigid ligand backbone systems (e.g., chiraphos and binap), in which the steric interactions of the backbone groups lead to a strongly preferential backbone configuration, the configuration is maintained throughout the conformational search. Thus, for a particular backbone system, the values of α and β remain within a fairly narrow range as the ϕ and ψ torsion angles vary. However, for ligands that produce seven-membered rings on binding to the metal (e.g., diop, a-dmabppm, b-dmabppm, bppm), the backbone possesses considerably more flexibility, and it changes in accord with the torsional positions of the phenyl groups, as described further below.

In summary, our approach to determining the conformational space of the $[Rh(P\text{-}P^*)(nbd)]^+$ complexes reveals that for all the ligands studied, there are multiple minima within a several kcal mol^{-1} in energy of the global energy minimum. The number of distinct conformational minima is three for norphos and four for all other ligands (Figure 13).

Determination of the Conformational Minima in $[Rh(P\text{-}P^*)(nbd)]^+$ Complexes With cClus-A

The conformational space of $[Rh(\text{chiral diphosphine})(nbd)]^+$ was derived as follows (see above). The structure was built in Cerius[2] and an

unconstrained Monte Carlo search of the four phenyl ring ϕ and ψ torsional degrees of freedom was performed which generated 2,000 structures.

The data set derived above was then submitted to cClus-A without further conditioning and typical results illustrated in Figure 18. The conformational data obtained from the Monte Carlo search used as input for cClus-A has well defined clusters so no conditioning was needed (Figures 18-27).

From Figure 18, we see several important features: the torsion angle plot shows perfect redundancy modulo 180°, which is expected since there is a C_2 axis through the P-aryl bond. It is evident from Figure 18 that cClus-A unambiguously identifies at least one structure in each important cluster.

Determination of conformational space was performed on the following diphosphine ligands as described above; binap, chiraphos, a-dmabppm, b-dmabppm, bppm, diop, dmabppm, dpc, dpcb, and norphos (Figures 13). The data set obtained form each complex was submitted to cClus-A for cluster analysis. Plots of torsion 1 versus torion 2 and torsion 3 versus torsion 4 are shown in Figure 18 through Figure 27. In a few of the torsion plots, there is a cluster that is not identified by cClus-A. All of these clusters missed, except one, exist outside of a difference of 10 kcal mol^{-1} of the global minimum energy. These clusters then are of little importance according to a Boltzman weight calculation. Only one data set, chiraphos, contains clusters that exist within 10 kcal mol^{-1} of the global energy minimum that were not identified by

cClus-A. The clusters which were not identified have torsion angle values of about ϕ_a = -30°, ϕ_b = 30°, ψ_a = -90°, and ψ_b = 90° (each cluster has roughly the same values for each torsion angle due to the C_2 axis of phenyl rings, i.e. -90° is equal to +90°). These values are represented in another cluster that was detected by cClus-A; ϕ_a = -35.3°, ϕ_b = 28.6°, ψ_a = -85.3°, and ψ_b = -87.1°.

The efficiency of cClus-A is shown with this diphosphine Rhodium system containing four torsion angles by unambiguously detecting each cluster that is derived form the Monte-Carlo conformational search. The clusters that were not detected by cClus-A are either (1) of high energy that would not exist according to a Boltzman calculation or (2) are detected in another cluster(s) when torsion angles are compared with conditioning due to the C_2 axis of phenyl rings.

Computational Methods

All calculations were performed on a Silicon Graphics Iris Indigo R3000, Silicon Graphics Iris Indigo^2 R4400, Silicon Graphics Iris Indigo^2 R10000, IBM RS/6000 Model 59H, IBM RS/6000 Model 3AT workstation, or Silicon Graphics PowerChallenge array using Cerius^2 1.6, 3.0, and 4.5.[16] An MM2 type force field was employed with modifications listed in Table 10 and the literature.[7,14,24-26,63,64]

Energy minimization was carried out using the Conjugate Gradient 200 minimizer with a step size of 2.00 Å and a termination criterion of 0.100

kcal.mol^{-1} Å^{-1} or a Fletcher-Powell minimizer with a step size of 2.00 Å and a termination criterion of 0.0100 kcal mol^{-1} Å^{-1} unless otherwise noted. Because the emphasis in this work is on intramolecular steric interactions, and because these vary largely as a result of phenyl group torsional orientations, no attempt was made to include partial charge distributions, or to model the role of solvent.[66]

Force-Field Parameterization

Parameters for the [Rh(P-P*)(nbd)]$^{+}$ system were modified from those presented in the literature.[7,14,24-26,63,64] Computed structures were compared against crystal structure data as well as data reported previously and the results are listed in Table 11.[7,14,24-26,63,64,66]

The bound olefin was modeled as described previously.[7] A dummy atom (D1 and D2) is placed at the center of the C=C bond slightly displaced from the bond axis. The dummy atom is directly bonded to the metal. Each carbon atom is also bonded to the metal to ensure each atom is numbered correctly with respect to non-bonded interactions. The Rh-C(olefin) force constants are all set to zero. These "ghost bonds" are present only to ensure a correct topology.[7]

Each dummy atom and phosphorus atom needs to be labeled uniquely since one P-Rh-D angle is 90° and the other 180°. By convention D1 is placed *trans* to P_b. To ensure the torsion angles are defined in precisely the same

way for each comparison within a set of structures, the atom numbers corresponding to Rh-P-C-C were used. In molecular dynamics runs, the lone pairs of electrons and dummy atoms were given a fictitious mass of 12 to ensure stability in the calculations.

Table 1. Comparison of Experimental and Computed Bond Distances (in Å), Angles (°), and Torsion Angles (°) for $[(\eta^5\text{-}C_5H_5)Re(\eta^2\text{-}\alpha\text{-olefin})(NO)(PPh_3)]^+$ Complexes Generated with MM, SEQM, and DFT (BOP/DNP) Methods

Bond Length or Angle	X-Ray[31]	Number of Data Points in CSD	MM Structure[9]	SEQM Structure[19]	DFT Structure
Re-Cp (centroid)	1.95(3)	199		2.00(1)	2.05(1)
Re-Cp ring C	2.29(4)	199	2.04(9)		
Re-P	2.43(5)	1806	2.53(1)	2.47(1)	2.53(1)
Re-N	1.76(4)	207	1.992(1)	1.81(2)	1.781(2)
Re-CH_2 (olefin)	2.24(7)	56	2.00(4)	2.08(1)	2.26(2)
Re-C_{ipso} (olefin)	2.26(10)	56	2.28(4)	2.10(2)	2.34(4)
Re-Centroid (olefin)	2.13(8)	56	2.04(2)	1.95(1)	2.19(2)
N-O	1.19(3)	207	1.10	1.204(2)	1.193(1)
C=C	1.41(4)	56	1.389(1)	1.499(3)	1.427(4)
Re-N-O	174(3)	207	179.3(4)	169(2)	172(2)
Re-C(olefin centroid)-C_{ipso}	91(1)	9		90.8(9)	94(2)
Re-C(olefin centroid)-C_{ipso}-P	-2(16)	9		-175(2), 9(5)	-172(4), 9(5)

Table 2. Single Point DFT/DNPP Energies (in kcal/mol) Relative to the Lowest Energy Isomer Computed for Different Functionals

Olefin Substituent	Isomer (Figure 2)	B3LYP	BLYP	BP	BOP
Me	*RS,SR*	0	0	0	0
	*RS,SR*2	3.576	3.838	3.849	3.636
	RR,SS	3.438	2.102	3.014	2.858
	*RR,SS*2	5.255	5.382	6.228	6.112
Bn	*RS,SR*		0	0	0
	*RS,SR*2		4.369	4.862	4.727
	RR,SS		1.275	2.789	2.723
	*RR,SS*2		5.459	6.608	6.426
i-Pr	*RS,SR*		0	0	0
	*RS,SR*2		3.947	4.390	3.655
	RR,SS		3.022	2.738	2.779
	*RR,SS*2		6.906	5.573	5.477

Table 3. DFT (BOP/DNP) Optimized Energies (in kcal/mol) Relative to the Lowest Energy Isomer for All Isomers of the $[(\eta^5\text{-}C_5H_5)Re(\eta^2\text{-}CH_2{=}CHR)(NO)(PPh_3)]^+$ Complexes Following Molecular Mechanics Grid Search, Torsion Angles (in degrees) for Both the Partially UFF-Optimized and Fully BOP/DNP-Optimized Structures. (Redundant Conformations are Italicized)

R	Isomer (Figure 2)	Isomer Label	Relative BOP/DNP Energy	Torsion Angle 1 Predicted by MM	Torsion Angle 2 Predicted by MM	Torsion Angle 1 Found by DFT	Torsion Angle 2 Found by DFT
Bn	*RS,SR*	**A**	0.00	65.7	68.6	94.9	88.2
		B	0.23	-176.2	64.4	-168.2	115.5
		C	*0.38*	*-167.7*	*-71.9*	*-167.6*	*-65.4*
		D	4.40	-78.7	-85.6	95.0	-91.0
	*RS,SR*2	**A**	0.00	74.2	69.5	77.2	80.1
		B	0.56	161.7	-70.0	91.9	-59.9
		C	2.69	-78.0	87.1	-20.8	73.2
	RR,SS	**A**	0.00	-66.0	-68.3	-82.9	-77.6
		B	1.60	174.0	68.4	171.0	41.1
		C	3.67	77.0	-91.1	19.2	-68.4
	*RR,SS*2	**A**	0.00	97.8	-65.0	-79.8	-77.7
		B	0.04	-173.7	59.5	-89.8	45.3
		C	*0.16*	*-69.5*	*-68.3*	*-81.4*	*-82.5*
Ph	*RS,SR*	**A**	0.00	-68.2		-9.7	
		B	*0.01*	*65.0*		*-9.5*	
	*RS,SR*2	**A**	0.00	18.6		-13.6	
		B	*0.03*	*-90.0*		*-16.5*	
	RR,SS	**A**	0.00	-80.0		-173.2	
	*RR,SS*2	**A**	0.00	-70.0		-151.4	
i-Pr	*RS,SR*	**A**	0.00	-47.2		-38.2	
		B	2.54	174.0		-130.8	

		C	3.77	43.9		89.1	
	*RS,SR*2	**A**	0.00	-179.9		-153.6	
		B	1.85	-27.2		-41.9	
		C	2.61	-57.1		-67.7	
		D	4.98	107.5		58.2	
		E	*5.68*	*45.8*		*59.7*	
	RR,SS	**A**	0.00	51.6		45.7	
		B	0.24	132.6		137.3	
		C	3.71	-83.1		-85.9	
	*RR,SS*2	**A**	0.00	179.6		133.8	
		B	1.82	50.0		87.7	
		C	6.28	-45.6		-63.0	
n-Pr	*RS,SR*	**A**	0.00	70.7	178.3	90.6	-179.8
		B	1.17	-172.0	178.8	-166.4	-177.0
		C	1.18	66.0	66.7	86.5	66.8
		D	1.23	82.9	-72.9	94.7	-72.4
		E	2.45	-167.8	-74.3	-164.4	-69.5
		F	3.52	-80.5	179.0	-8.4	174.5
		G	*3.54*	*-87.9*	*-76.2*	*-9.9*	*178.6*
		H	4.52	-173.7	68.7	-179.4	84.2
		I	5.17	-91.5	84.1	-4.9	81.7
	*RS,SR*2	**A**	0.00	177.8	177.0	81.2	179.8
		B	*1.17*	*72.3*	*178.0*	*79.3*	*178.9*
		C	2.52	85.6	-71.4	88.6	-68.5
		D	2.61	71.2	69.1	75.2	72.6
		E	4.83	-61.8	-161.3	-25.9	177.4
	RR,SS	**A**	0.00	-70.8	-178.2	-92.8	179.9
		B	0.58	-160.3	-60.1	-93.3	-71.8
		C	*0.98*	*-65.7*	*-66.5*	*-88.7*	*-71.8*

	D	1.27	-83.2	72.9	-94.4	73.0
	E	2.74	173.7	-178.7	175.3	171.4
	F	*3.71*	*82.1*	*-168.3*	*3.2*	*-176.7*
	G	4.03	169.5	72.8	176.8	74.4
*RR,SS*2	**A**	0.00	-72.3	-177.9	-77.5	-179.1
	B	*0.12*	*-158.7*	*-166.9*	*-81.8*	*179.2*
	C	1.09	-70.0	-70.0	-75.6	-69.4
	D	1.46	-160.0	80.0	-90.2	72.9
	E	*1.47*	*-84.8*	*72.0*	*-90.6*	*72.7*
	F	*1.50*	*174.1*	*59.9*	*-87.0*	*73.3*
	G	3.93	67.6	165.9	21.8	-174.0

Table 4. Single Point BOP/DNPP Energies (in kcal/mol) Relative to the Lowest Energy Isomer, and Ligand Repulsive Energies, $E''_R{}^{DFT}$ in kcal/mol, for the α-Olefins in the $[(\eta^5\text{-}C_5H_5)Re(NO)(PPh_3)]^+$ Environment

Olefin Substituent	Isomer (Figure 2)	Relative BOP/DNPP Energy	$E''_R{}^{DFT}$
Me	*RS,SR*	0	39.9
	*RS,SR*2	3.636	51.4
	RR,SS	2.858	55.1
	*RR,SS*2	6.112	56.4
Bn	*RS,SR*	0	40.9
	*RS,SR*2	4.727	50.9
	RR,SS	2.723	53.8
	*RR,SS*2	6.426	59.5

i-Pr	*RS*,*SR*	0	54.0
	RS,*SR*2	3.655	50.5
	RR,*SS*	2.779	57.0
	RR,*SS*2	5.477	68.8
Ph	*RS*,*SR*	0	45.9
	RS,*SR*2	4.388	68.8
	RR,*SS*	0.634	65.2
	RR,*SS*2	7.633	57.6
n-Pr	*RS*,*SR*	0	41.4
	RS,*SR*2	9.101	55.0
	RR,*SS*	6.31	60.9
	RR,*SS*2	6.586	58.1
t-Bu	*RS*,*SR*	0	52.4
	RS,*SR*2	10.239	68.9
	RR,*SS*	7.108	72.2
	RR,*SS*2	12.854	78.3
$SiMe_3$	*RS*,*SR*	0	45.1
	RS,*SR*2	6.445	58.5
	RR,*SS*	5.362	62.0
	RR,*SS*2	13.135	58.9

Table 5. Molecular Mechanics Based Diastereoselectivities, de_{MM}, Based on All Unique Conformers Reported in Table 4 and Experimental Diastereoselective Excess Values, *de*,[13] for the Stereoselective Binding of α-Olefins to $[(\eta^5\text{-}C_5H_5)Re(NO)(PPh_3)]^+$

α-Olefin	de_{MM}	de^{13}
CH_2=CHMe	1.0	0.95
CH_2=CHBn	0.003	0.88
CH_2=CH(*i*-Pr)	0.11	0.99
CH_2=CHPh	1.0	0.93
CH_2=CH(*n*-Pr)	0.0	0.94
CH_2=CH(*t*-Bu)	1.0	0.73
CH_2=$CHSiMe_3$	1.0	0.63

Table 6. Ligand Repulsive Energies (in kcal/mol) Computed From BOP/DNP Optimized Structures, E″R, Boltzmann Weighted Ligand Repulsive Energies, <E″R>, (in kcal/mol), Computed Diastereoselectivities, and Experimental Diastereoselectivities for the [(η5-C5H5)Re(η2-CH2=CHR)(NO)(PPh3)]+ Complexes

R	Isomer (Figure 2)	Isomer Label (Table 3)	E''_R	$\langle E''_R \rangle$	de_{DFT}	de^{13}
Me	*RS,SR*		39.9	1.0	0.99	0.95
	*RS,SR*2		51.4	7.7×10^{-12}		
	RR,SS		55.1	5.5×10^{-14}		
	*RR,SS*2		56.4	2.3×10^{-17}		
t-Bu	*RS,SR*		52.4	1.0	1.0	0.73
	*RS,SR*2		68.9	2.8×10^{-20}		

	RR,SS		72.2	1.9×10^{-20}		
	*RR,SS*2		78.3	4.0×10^{-29}		
$SiMe_3$	*RS,SR*		45.1	1.0	1.0	0.63
	*RS,SR*2		58.5	2.7×10^{-15}		
	RR,SS		62.0	4.2×10^{-17}		
	*RR,SS*2		58.9	1.8×10^{-20}		
Bn	*RS,SR*	**A**	40.5	0.4	0.81	0.88
		B	48.2	4.1×10^{-7}		
		D	40.5	0.4		
	*RS,SR*2	**A**	51.9	7.2×10^{-13}		
		B	58.1	6.3×10^{-18}		
		C	68.1	4.4×10^{-27}		
	RR,SS	**A**	52.9	3.9×10^{-12}		
		B	70.0	7.4×10^{-26}		
		C	64.8	10.0×10^{-24}		
	*RR,SS*2	**A**	55.5	5.7×10^{-17}		
		B	61.8	1.3×10^{-22}		
Ph	*RS,SR*	**A**	46.4	0.8	0.77	0.93
	*RS,SR*2	**A**	66.8	5.4×10^{-19}		
	RR,SS	**A**	64.2	2.1×10^{-14}		
	*RR,SS*2	**A**	62.0	7.4×10^{-18}		
i-Pr	*RS,SR*	**A**	45.7	1.0	0.99	0.99
		B	48.2	0.0		
		C	51.9	4.8×10^{-8}		
	*RS,SR*2	**A**	49.4	2.2×10^{-9}		
		B	51.0	7.4×10^{-12}		

		C	51.4	8.6×10^{-13}		
		D	59.8	1.1×10^{-20}		
	RR,SS	**A**	59.5	1.4×10^{-15}		
		B	55.0	1.5×10^{-12}		
		C	62.9	6.0×10^{-21}		
	*RR,SS*2	**A**	70.0	1.3×10^{-25}		
		B	63.7	3.5×10^{-22}		
		C	73.5	8.5×10^{-33}		
n-Pr	*RS,SR*	**A**	40.8	0.7	0.79	0.94
		B	42.4	0.0		
		C	41.8	0.0		
		D	40.9	0.1		
		E	43.9	6.7×10^{-5}		
		F	44.0	9.6×10^{-6}		
		H	43.9	1.8×10^{-6}		
		I	43.4	1.2×10^{-6}		
	*RS,SR*2	**A**	51.3	1.4×10^{-11}		
		C	51.0	2.3×10^{-13}		
		D	47.9	4.1×10^{-11}		
		E	56.4	5.4×10^{-19}		
	RR,SS	**A**	53.5	4.5×10^{-12}		
		B	53.7	1.0×10^{-12}		
		D	53.7	4.0×10^{-13}		
		E	61.5	6.2×10^{-20}		
		G	63.9	1.1×10^{-22}		
	*RR,SS*2	**A**	57.4	6.2×10^{-18}		

C	57.8	4.5×10^{-19}
D	61.2	8.0×10^{-22}
G	64.6	3.9×10^{-26}

Table 7. Torsion Angles (in Degrees) Generated by Inspection and Using SAS for the *RR,SS* Isomer of $[(\eta^5\text{-}C_5H_5)Re(\eta^2\text{-}CH_2{=}CHR)(NO)(PPh_3)]^+$ Complexes Following Molecular Mechanics Grid Search for Both Partially UFF-Optimized Structures.

R	Isomer (Figure 4)	Analysis by Inspection (Chapter 2)		SAS k-Means Clustering	
		Torsion 1	Torsion 2	Torsion 1	Torsion 2
n-Pr	*RR,SS*	173.7	-178.7	173.7	-178.7
		169.5	72.8	169.5	72.8
		-83.2	72.9	-83.2	72.9
		-70.8	-178.2	N/A	N/A
		-160.3	-60.1	-160.3	-60.1
				60.4	169.4
				95.2	-72.5

Table 8. Torsion Angles (in Degrees) Generated by Inspection and Using cClus-A the *RS,SR*2 Isomer of $[(\eta^5\text{-}C_5H_5)Re(\eta^2\text{-}CH_2{=}CHR)(NO)(PPh_3)]^+$ Complexes Following Molecular Mechanics Grid Search for Both Partially UFF-Optimized Structures.

R	Isomer (Figure 4)	Analysis by Inspection (Chapter 2)		Graph Theory Analysis	
		Torsion 1	Torsion 2	Torsion 1	Torsion 2
n-Pr	*RR,SS*	173.7	-178.7	170.1	-180.0
		169.5	72.8	170.0	70.0
		-83.2	72.9	-80.1	70.1
		-70.8	-178.2	-70.0	-180.0
		-160.3	-60.1	-160.3	-60.1
				-69.9	-70.0

Table 9. Torsion Angles (in Degrees) Generated from cClus-A of the Torsional Space of $[(\eta^5\text{-}C_5R_5)Re(\eta^2\text{-}CH_2{=}CHR')(NO)(PMe_3)]^+$ Complexes Following Molecular Mechanics Grid Search for Partially UFF-Optimized Structures.

R	R′	Isomer (Figure 4)	Torsion 1	Torsion 2
H	Bn	*RS,SR*	-174.9	70
			85.0	65.0
			95.1	-70.0
			-165.0	-65.0
		*RS,SR*2	75.0	-90.2
			70.0	65.0

		RR,SS	-90.1	75.0
			179.9	55.1
			-89.9	-70.0
		*RR,SS*2	-75.0	85.2
			-70.0	-65.0
H	*n*-Pr	*RS,SR*	-160.0	-75.0
			95.0	-70.0
			80.0	70.0
			-174.9	80.1
		*RS,SR*2	70.0	65.0
			90.0	-70.0
		RR,SS	-75.0	-70.0
			-85.0	70.0
			-170.0	-175.0
		*RR,SS*2	-75.0	-180.0
			-70.1	-70.0
			-80.1	75.0
Me	Bn	*RS,SR*	-170.1	-60.1
			85.0	65.0
			175.2	80.0
			95.0	-75.0
		*RS,SR*2	69.9	60.0

		75.1	-90.3
		145.1	-55.0
	RR,SS	-85.0	-70.0
		-90.0	75.0
	RR,SS2	-74.9	-65.0
		-75.1	85.2
n-Pr	*RS,SR*	-164.9	180.0
		-165.0	-75.1
		90.0	180.0
		95.0	-70.0
		85.0	-70.0
		85.0	70.0
	RS,SR2	70.0	65.0
		154.9	-70.0
		85.0	-75.0
	RR,SS	-89.9	-180.0
		-94.9	70.0
		-85.0	-70.0
	RR,SS2	-74.9	-175.0
		-70.1	-65.0
		-80.0	75.0

Table 10. Energies (in kcal mol^{-1}), torsion angles (in degrees)[a], and elevation angles (in degrees)[b] characteristic of the relatively low-energy conformers in [Rh(diphosphine)(nbd)]$^{+}$ complexes.

Diphosphine	Number	Energy	ϕ_a	ϕ_b	ψ_a	ψ_b	α_a	α_b	β_a	β_b
binap	1	45.5	15	65	-62	3	63	139	174	99
binap	2	45.5	3	-62	65	15	99	174	139	63
binap	3	49.1	13	-44	-44	13	83	156	156	83
binap	4	52.9	72	-65	24	18	127	177	120	53
chiraphos	1	48.6	86	25	25	87	137	105	104	136
chiraphos	2	50.2	-30	23	89	-90	124	105	117	137
chiraphos	3	50.2	-90	89	23	-30	137	117	105	124
chiraphos	4	50.7	-34	88	88	-33	125	116	115	124
a-dmabppm	1	76.6	-25	13	-90	-80	109	104	137	144
a-dmabppm	2	78.7	-33	87	-90	-31	119	133	126	113
a-dmabppm	3	80.2	-68	19	21	-83	127	104	117	143
a-dmabppm	4	84	-68	83	18	-27	136	131	109	116
b-dmabppm	1	78.6	-87	23	18	-84	148	107	100	142
b-dmabppm	2	80.9	-34	86	89	-28	124	139	121	107
b-dmabppm	3	82.1	-69	73	19	-30	136	123	109	122
b-dmabppm	4	88.1	-33	18	-88	82	78	116	167	131

bppm	1	65.6	-86	20	16	-81	139	106	106	144
bppm	2	67.1	-15	14	-87	-82	109	96	136	155
bppm	3	67.2	-23	86	89	-10	109	143	136	102
bppm	4	70.4	-84	85	8	26	153	166	94	80
diop	1	58	-83	86	23	-5	127	150	115	96
diop	2	59.3	-26	-90	-89	-11	111	144	133	102
diop	3	62.1	-10	22	87	-85	101	114	145	132
diop	4	63.8	-86	30	21	86	130	124	112	123
dmabppm	1	91.9	-18	18	89	-82	111	100	137	149
dmabppm	2	92.5	-89	23	18	-84	151	108	98	140
dmabppm	3	95.1	-34	85	89	-28	123	140	122	106
dmabppm	4	96.7	-67	78	19	-24	134	133	111	113
dpc	1	69.7	-26	21	86	-83	113	112	131	132
dpc	2	71.2	-28	-88	88	-24	115	143	127	103
dpc	3	71.2	-88	23	21	-85	143	115	104	128
dpc	4	74.2	-85	74	15	-23	144	128	104	115
dpcb	1	72.5	85	-83	12	-14	137	137	107	107

dpcb	2	72.6	-11	9	-85	87	104	104	139	139
dpcb	3	73.3	84	20	19	84	130	114	113	129
dpcb	4	73.3	-24	-82	-82	-22	115	131	128	112
norphos	1	84.6	-11	-87	-86	-12	100	136	137	100
norphos	2	86.7	-3	17	-87	89	94	118	143	120
norphos	3	87	89	-86	18	-7	120	141	118	96

[a] The ϕ, ψ torsion angles are defined by viewing down the C_{aryl}-P bond (Figure 2). A torsion angle of 0° has the *ortho* substituent eclipsing the Rh-P bond vector. A ccw rotation of the aryl group gives rise to a negative torsion angle. Since the torsion angles are modulo 180°, we list only those values that lie between -90° and +90° (e.g., ϕ = -95° ≡ ϕ = +85°).

[b] The α, β elevation angles represent the C_{aryl}-P-Rh-P torsion angle. We define the elevation angles as positive regardless of whether the phenyl group is "up" or "down".

Table 11. Force field parameters and comparison between crystal and computed structures for $[Rh(P\text{-}P^*)(nbd)]^+$ complexes.

Bond	**Force Constant**[c]	**Equilibrium Value**
Rh-P	200	2.22 Å
Rh-C(centroid)[d]	150	2.15 Å
P-Rh-P	45	107°
P-Rh-C(centroid)	45	98° or 160°
C(centroid)-Rh-C(centroid)	65	90°

Bond	X-Ray[53]	Computed
Rh-P1	2.31(3) Å	2.23 Å
Rh-P2	2.31(3) Å	2.16 Å
Rh-D1[d]	2.12(3) Å	2.06 Å
Rh-D2[d]	2.13(3) Å	2.05 Å
P1-Rh-P2	88(4)°	87°
P2-Rh-D2	97(4)°	100°
P2-Rh-D1	171(5)°	170°
D1-Rh-D2	79(8)°	71°
P1-Rh-D1	97(4)°	103°
P1-Rh-D2	170(5)°	173°

[e] Force constant units are kcal mol^{-1} $Å^{-2}$ for bond stretches and kcal mol^{-1} rad^{-2} for angle bends.

[f]Center of the olefin C=C bond.

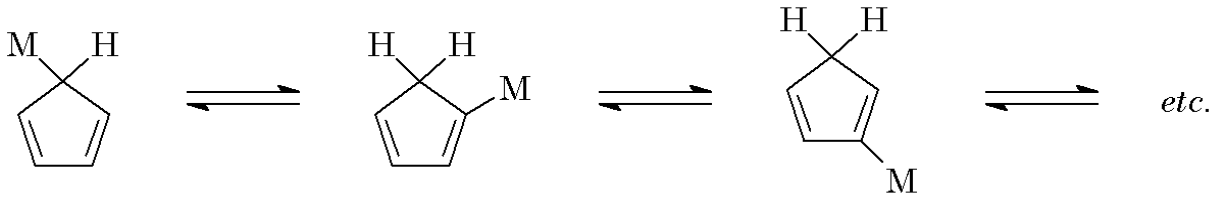

Figure 1. Example of metal migration about a cyclopentadienyl ring that is in an η^1 bonding arrangement with the metal.

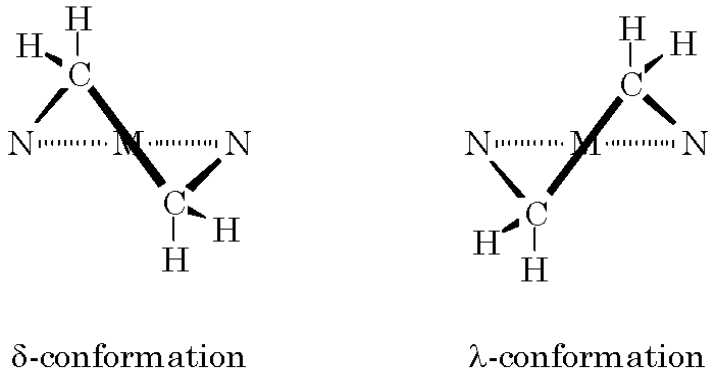

Figure 2. Chelate ring conformations observed for a bidentate ligand (in this case ethylene diamine is shown).

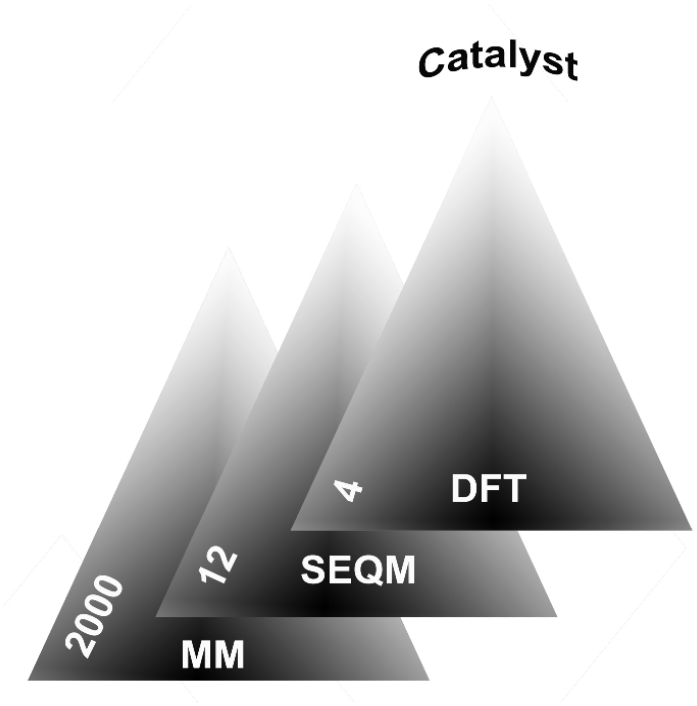

Figure 3. *De novo* design pyramid illustrating the successive applications of more sophisticated computational methods in order to refine a catalyst structure.

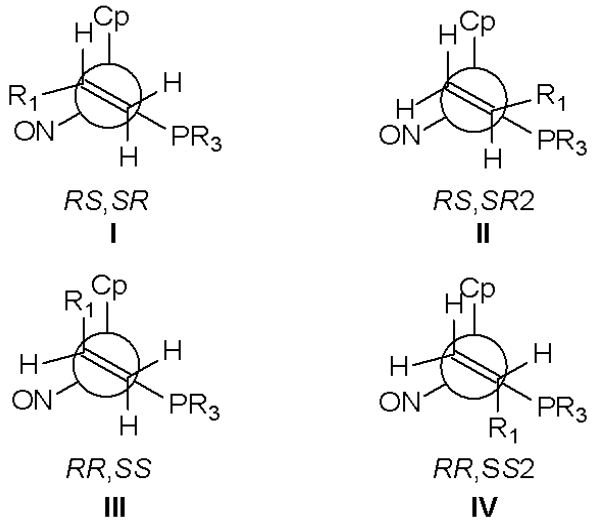

Figure 4. Four isomers of $[(\eta^5\text{-}C_5H_5)Re(\eta^2\text{-prochiral olefin})(NO)(PPh_3)]^+$. Structures I and II have the same olefinic face bound to the Re, as do isomers III and IV.

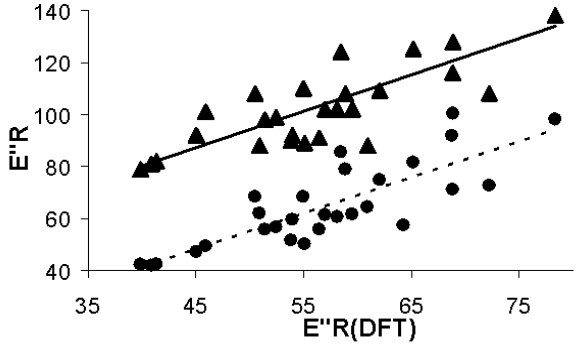

Figure 5. Plot of ligand repulsive energy, E''_R, from MM-optimized structure (triangles) and SEQM optimized structure (circles) versus E''_R computed from the DFT-optimized structure.

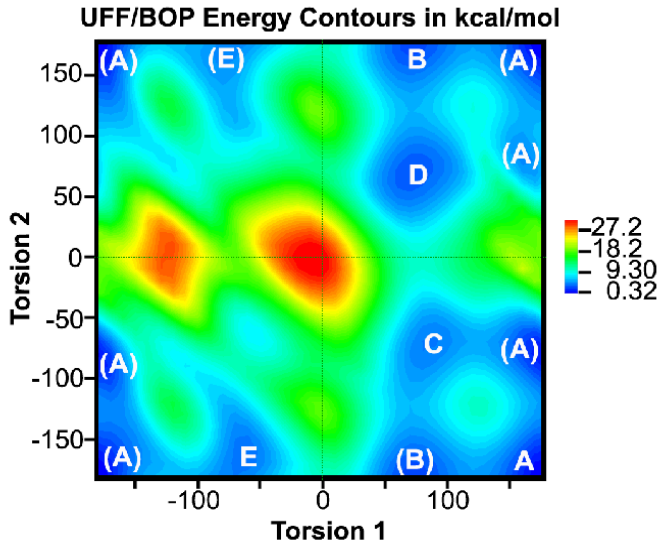

Figure 6. Grid search results on *RS*,*SR*2-[(η^5-C_5H_5)Re(η^2-1-butene)(NO)(PPh_3)]$^+$. The five low-energy unique isomers, A – E (Table 6), are generated by freezing all atoms in the molecule except those in the propyl substituent on the olefin. Redundant conformers are indicated in parentheses. (Low energy areas are shown as blue, high energy as red)

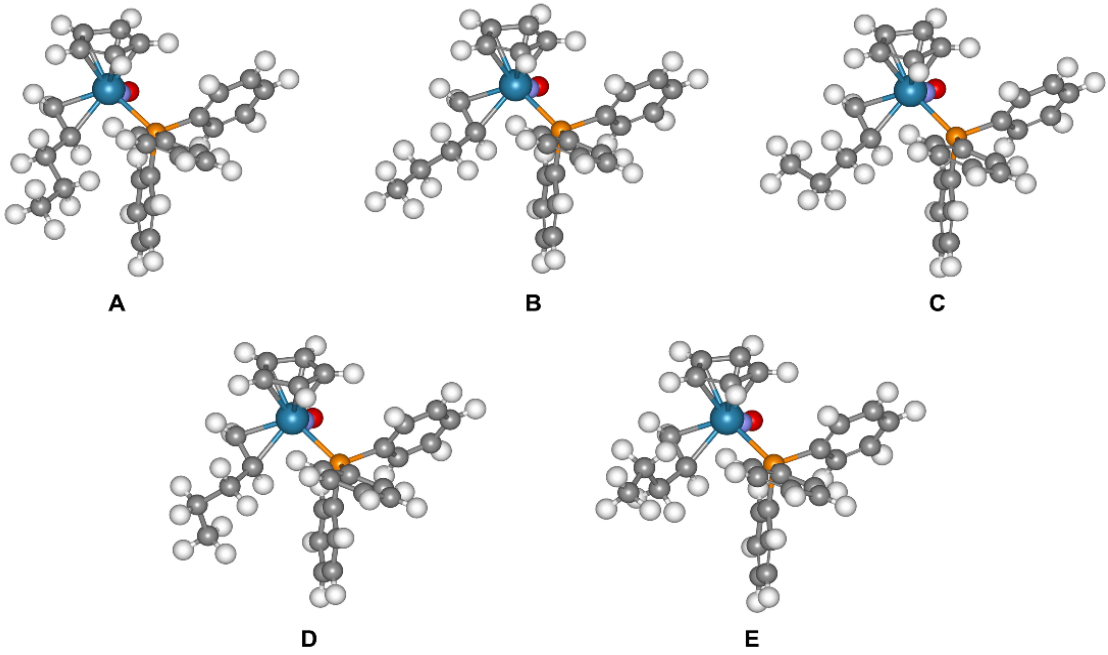

Figure 7. Five low-energy isomers, A – E (Table 4) generated from the DFT/MM conformational search on *RS,SR*2-[(η^5-C_5H_5)Re(η^2-1-butene)(NO)(PPh_3)]$^+$.

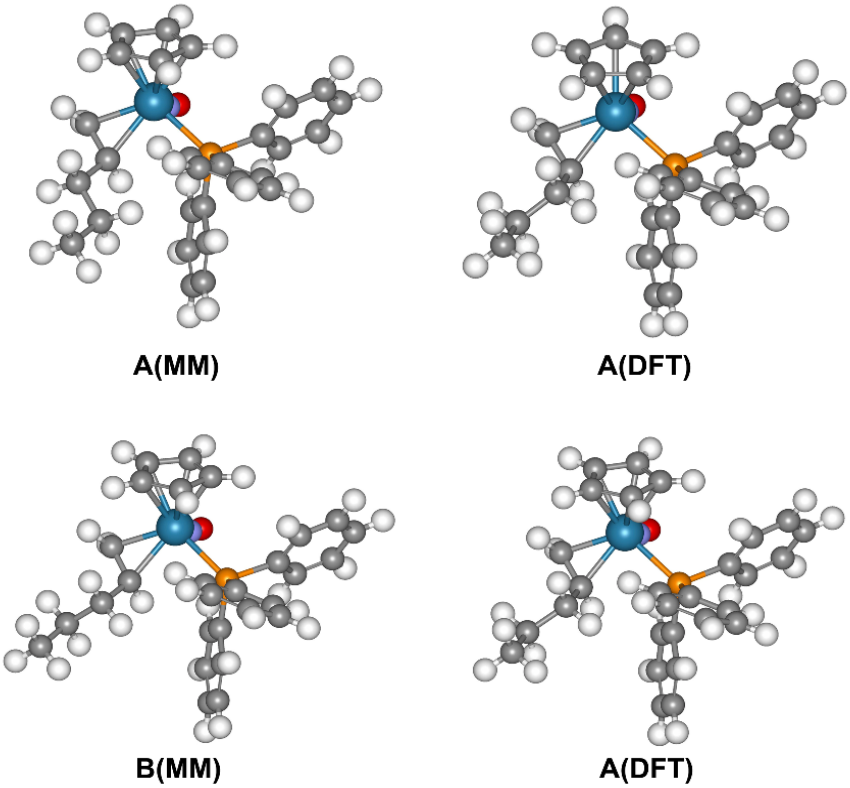

Figure 8. The two molecular mechanics minima, A(MM) and B(MM) for RS,SR2-[(η5-C5H5)Re(η2-1-butene)(NO)(PPh3)]+ (Table 4), collapse to a common minimum, A(DFT), after optimization with BOP/DNP. Note that the conformation of the propyl substituent on the olefin is the same in A(MM) and A(DFT).

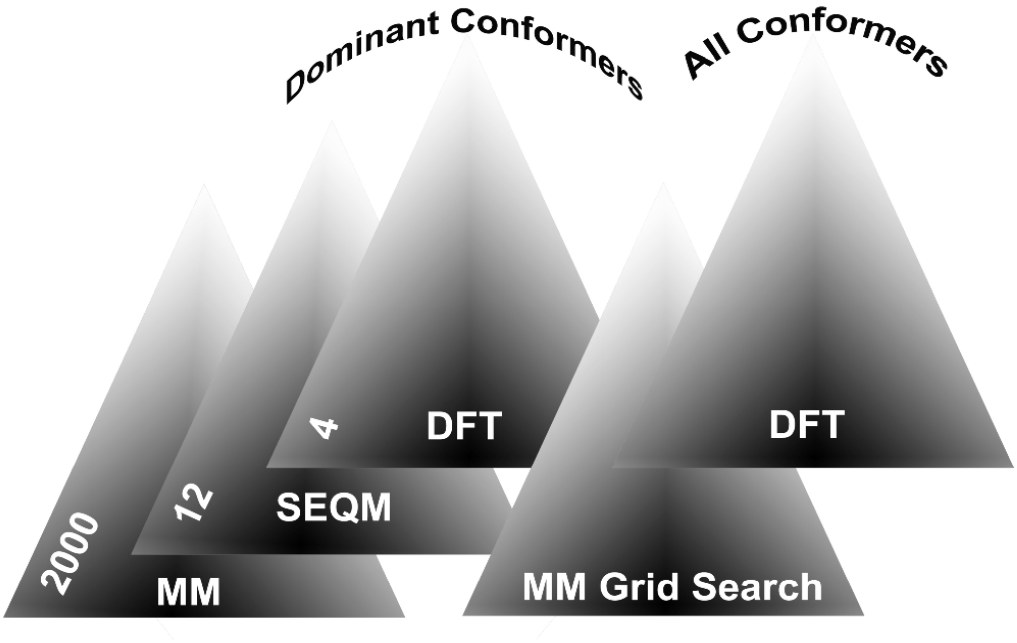

Figure 9. Modified *de novo* design pyramid illustrating the successive applications MM-SEQM-DFT-MM-DFT to identify all the conformers that can participate in the stereoselective olefin binding reaction.

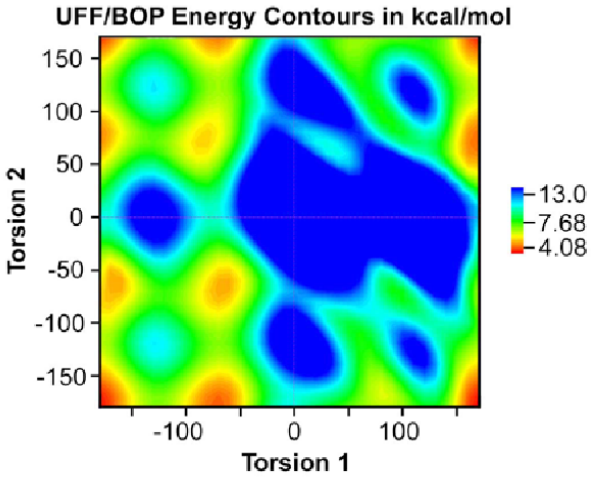

Figure 10. Grid search results on the *RR,SS*-[(η^5-C_5H_5)Re(η^2-1-butene)(NO)(PPh_3)]$^+$ isomer. (Low energy areas are shown as red spots, high energy as blue)

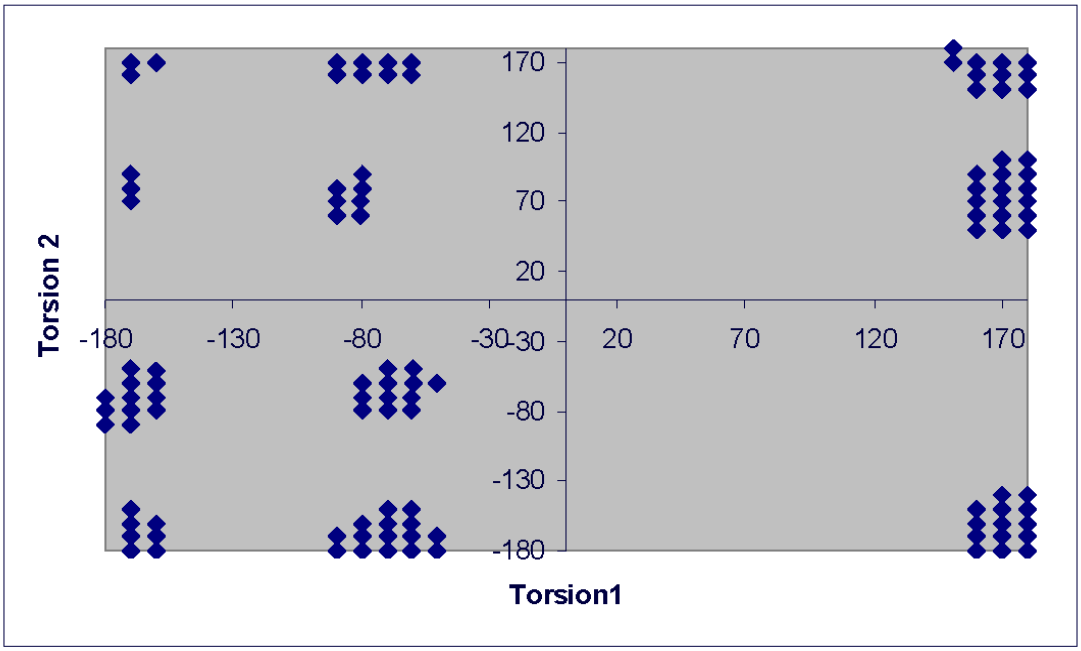

Figure 11. Conditioned data set of the *RR,SS*-[(η^5-C_5H_5)Re(η^2-1-butene)(NO)(PPh_3)]$^+$ isomer as used for input into cClus-A.

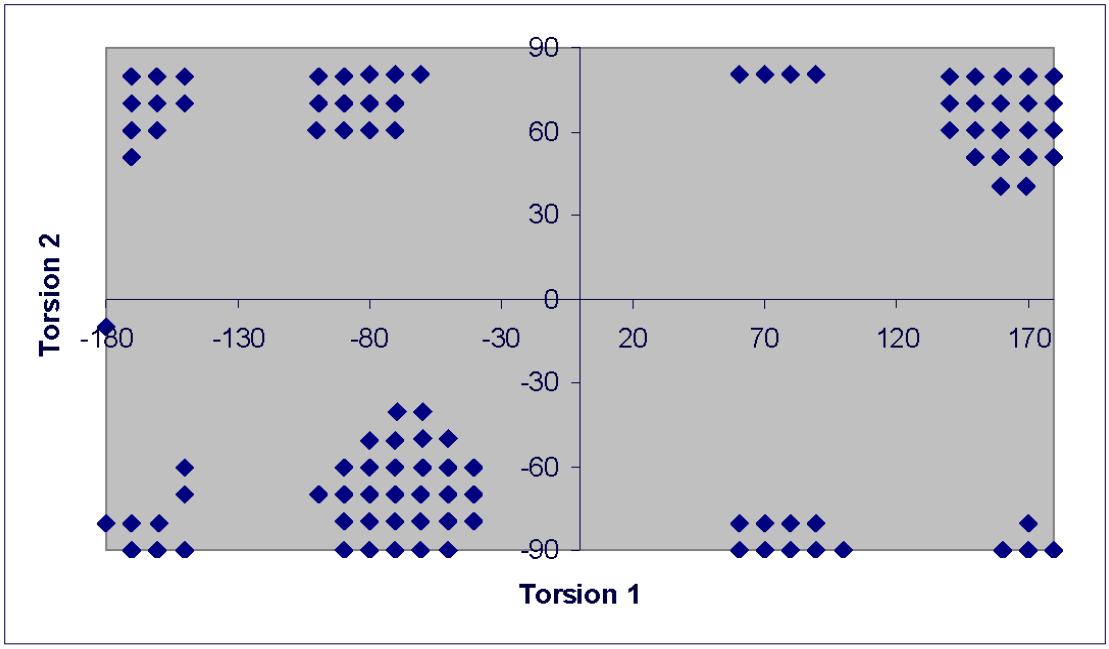

(a)

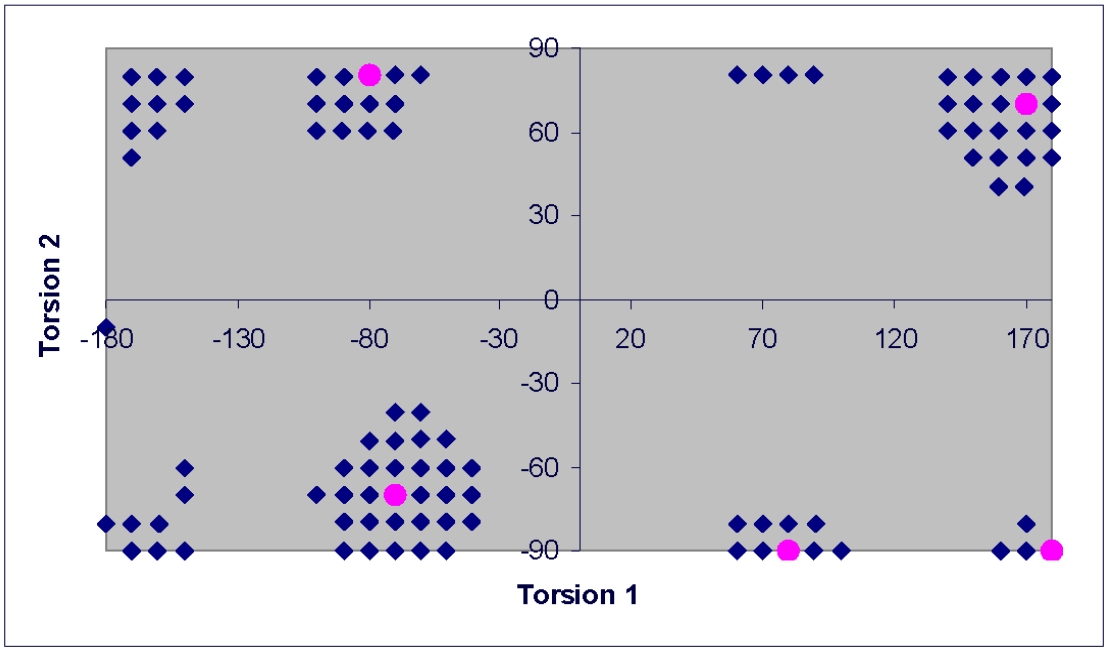

(b)

Figure 12. (a) Plot of conditioned data for the partially optimized grid search on the *RR,SS* isomer of $[(\eta^5\text{-}C_5H_5)Re(\eta^2\text{-}CH_2{=}CHBn)(NO)(PPh_3)]^+$. Torsion 1 is the C(olefin)=C(*ipso*)-CH_2-C(Ph) torsion angle, Torsion 2 is the C(*ipso*)-CH_2-C(Ph)-C(*ortho*) torsion angle. (b) The conditioned data are shown as blue diamonds whereas the cClus-A output is shown as pink circles.

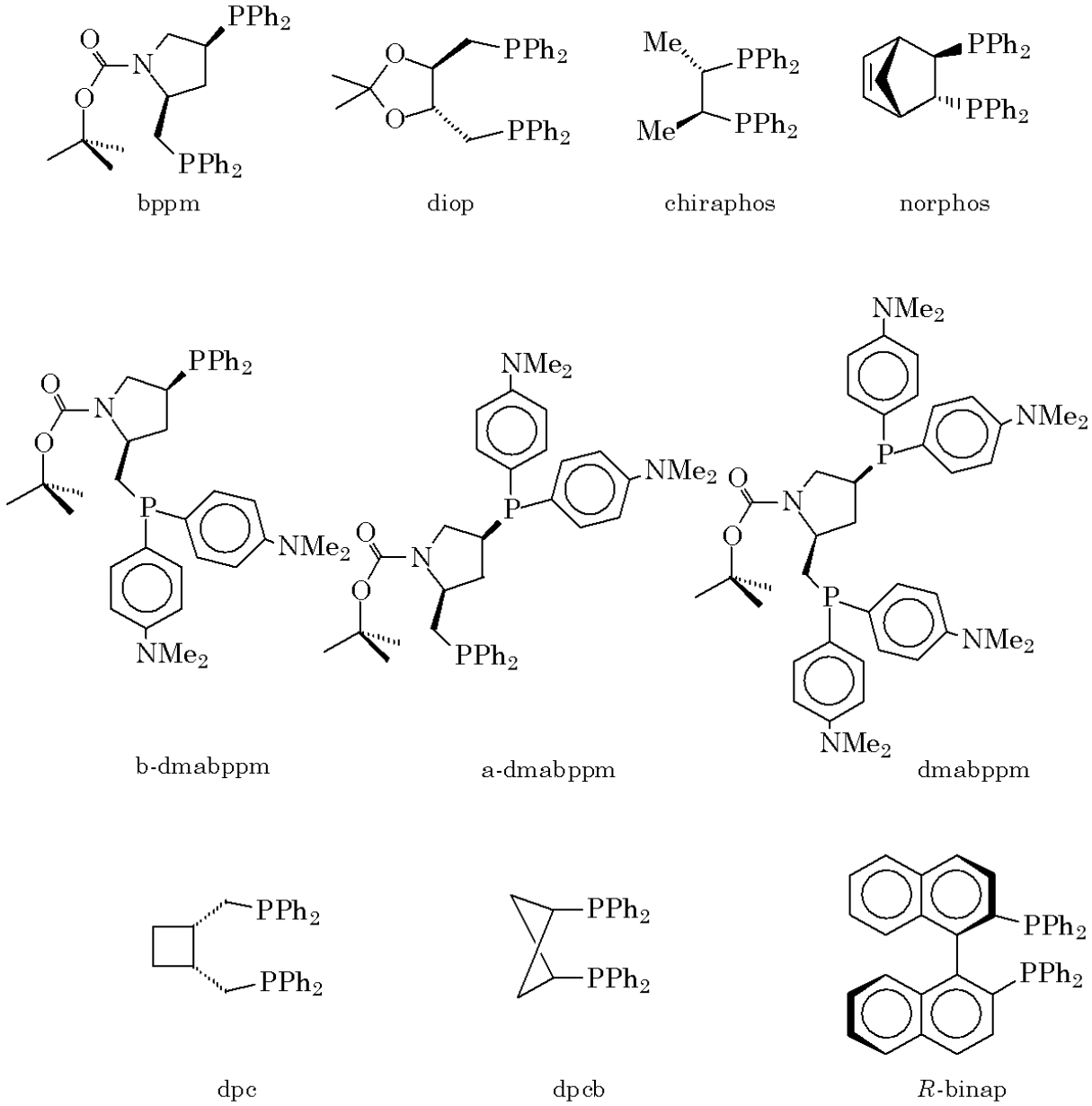

Figure 10. Examples of chiral bidentate phosphines used in asymmetric hydrogenation.

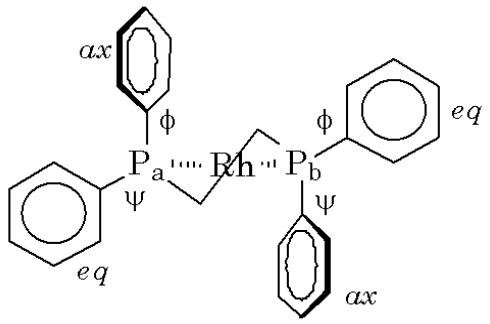

Figure 11. Definitions of torsion angles used in [(bidentate phosphine)Rh(substrate)]$^+$ complexes.

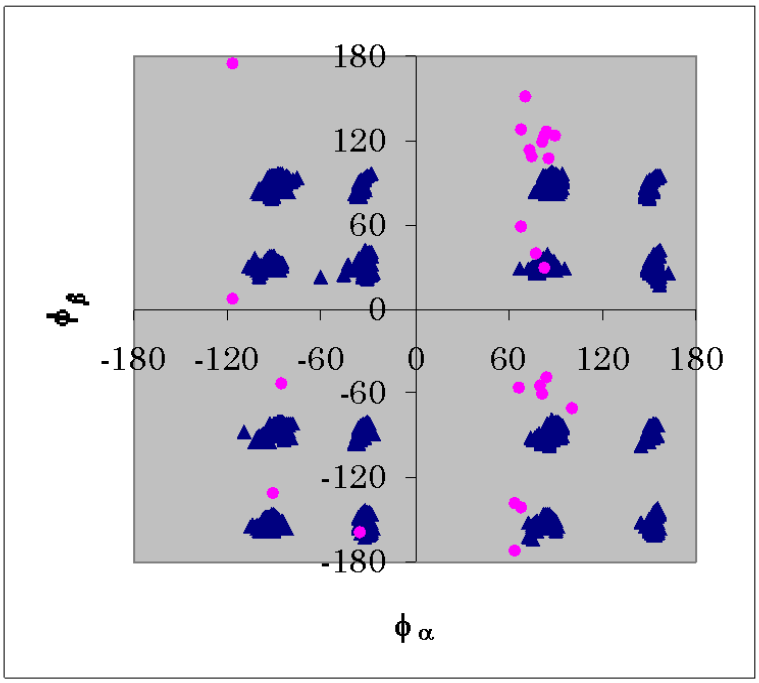

Figure 12. Plot of ϕ_b versus ϕ_a for [(chiraphos)Rh(nbd)]$^+$ generated as described in the text.

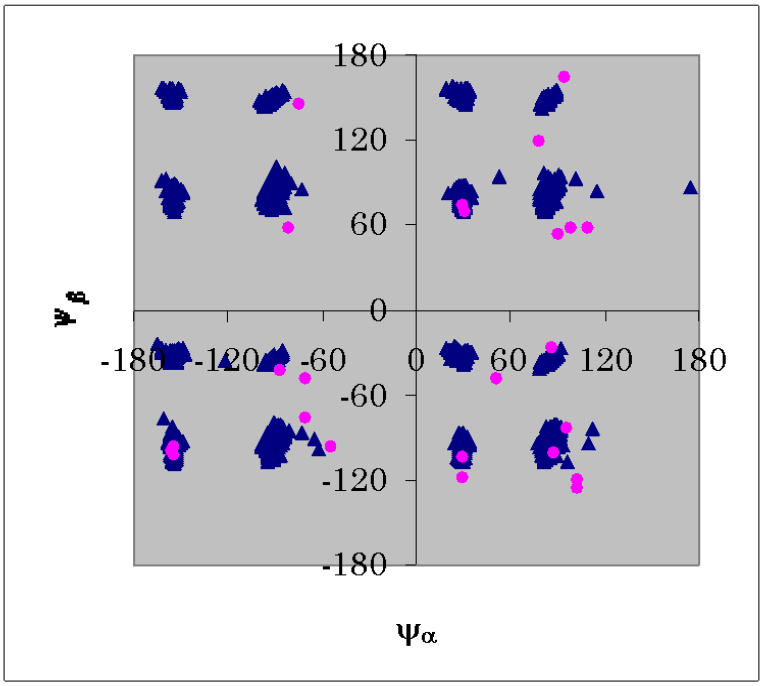

Figure 13. Plot of ψ_a versus ψ_b for [(chiraphos)Rh(nbd)]$^+$ generated as described in the text.

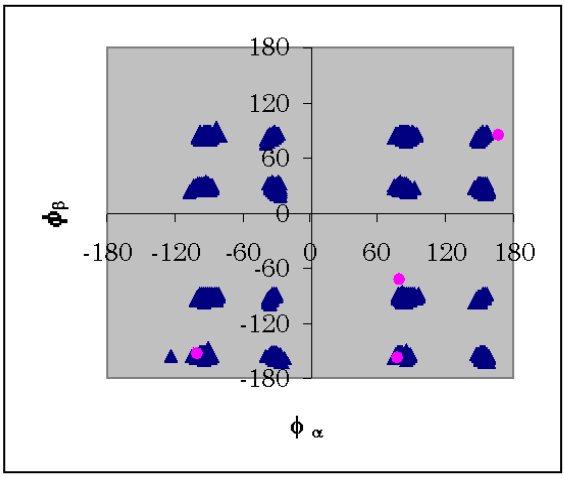

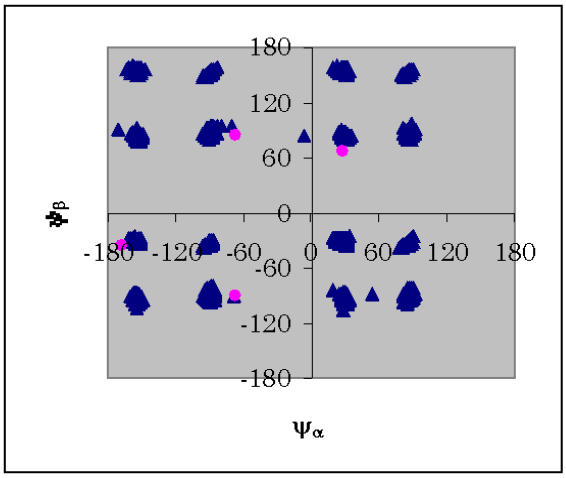

Figure 14. Plot of ϕ and ψ torsion angles for [(chiraphos)Rh(nbd)]$^+$ against each other after saddle points have been removed by Fletcher-Powell minimization. (Pink points are "allowable" unique low energy structures)

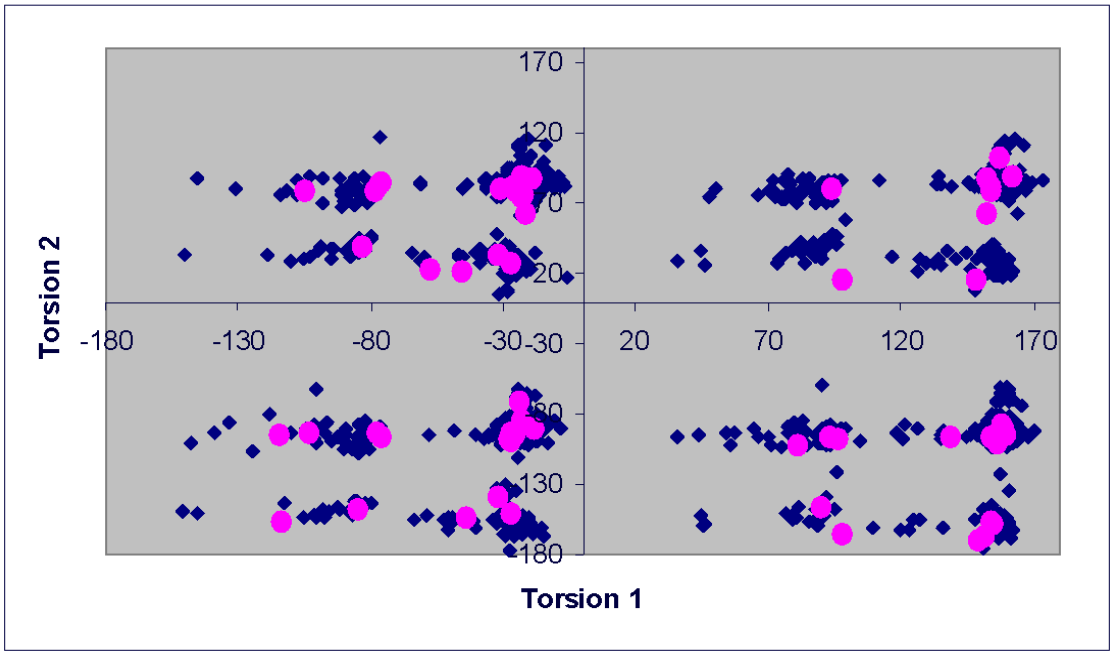

(a)

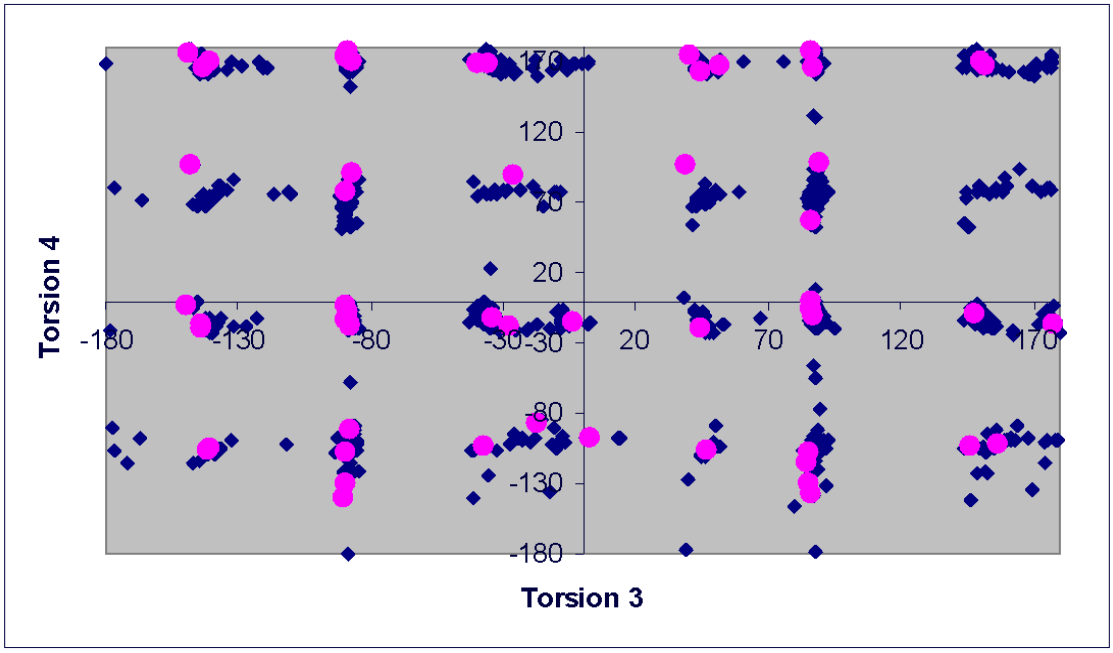

(b)

Figure 18. Plots of Torsion 1 versus Torsion 2 (a) and Torsion 3 versus Torsion 4 (b) for (ach2)Rh(nbd)]$^+$ showing conformational search data points (blue) overlaid with unique data points derived from cClus-A (pink).

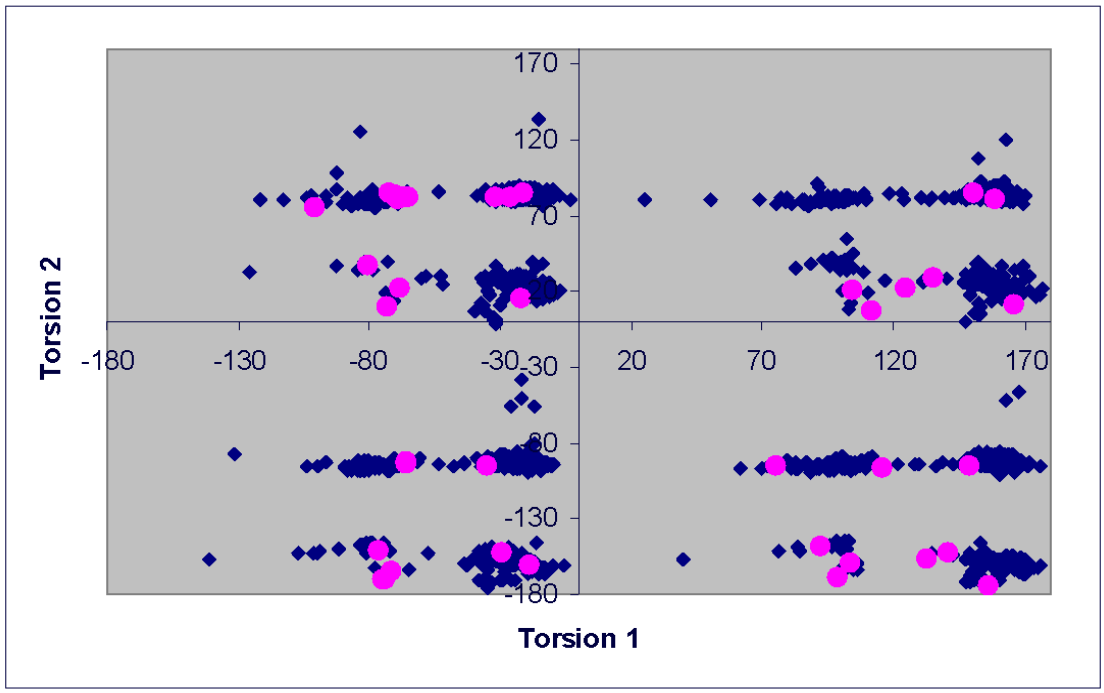

(a)

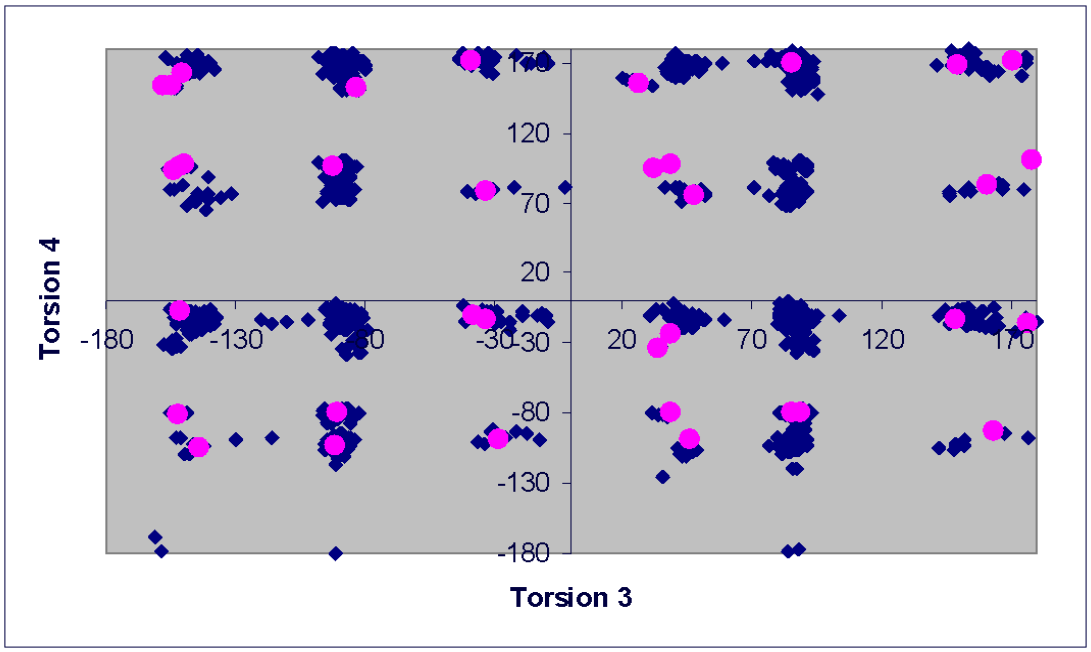

(b)

Figure 19. Plots of Torsion 1 versus Torsion 2 (a) and Torsion 3 versus Torsion 4 (b) for (ach3)Rh(nbd)]$^+$ showing conformational search data points (blue) overlaid with unique data points derived from cClus-A (pink).

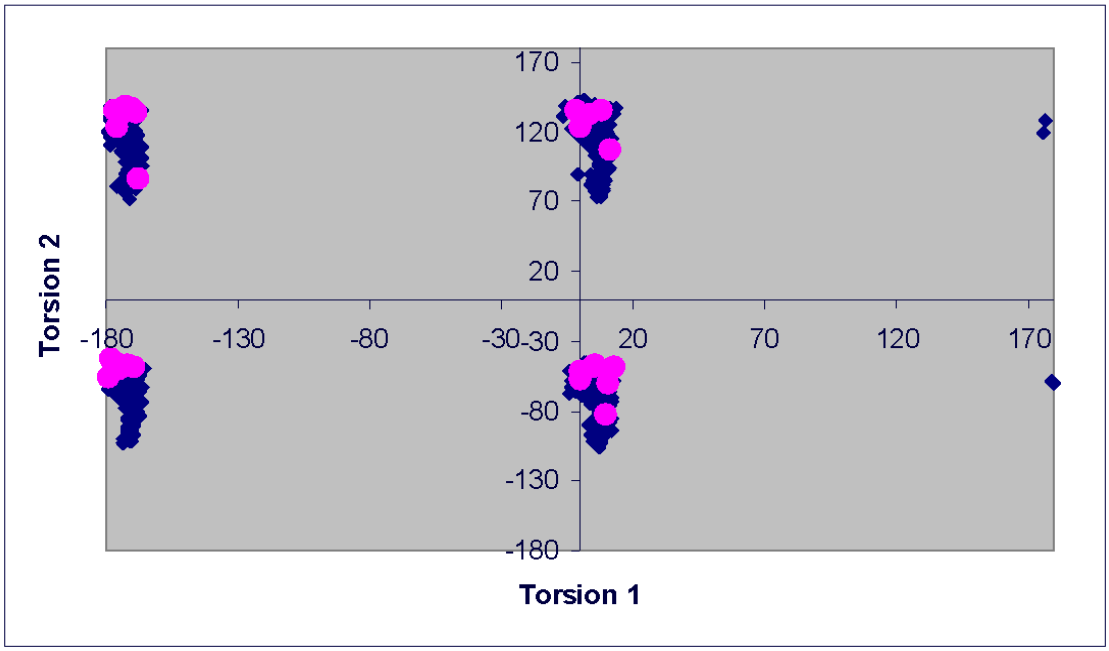

(a)

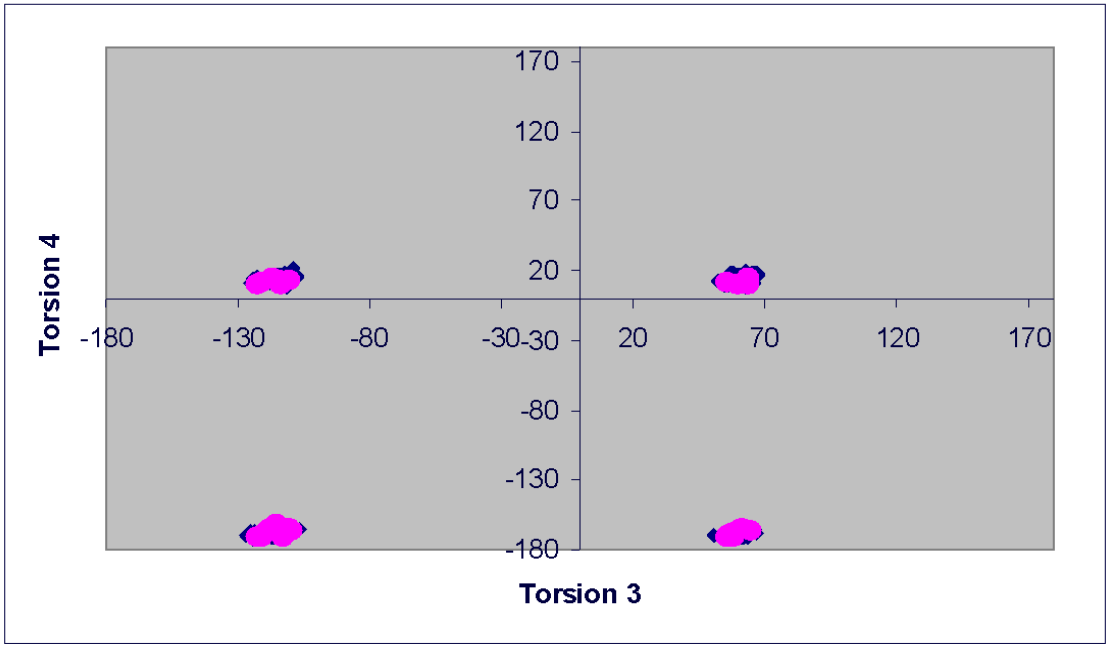

(b)

Figure 20. Plots of Torsion 1 versus Torsion 2 (a) and Torsion 3 versus Torsion 4 (b) for (binap)Rh(nbd)]$^+$ showing conformational search data points (blue) overlaid with unique data points derived from cClus-A (pink).

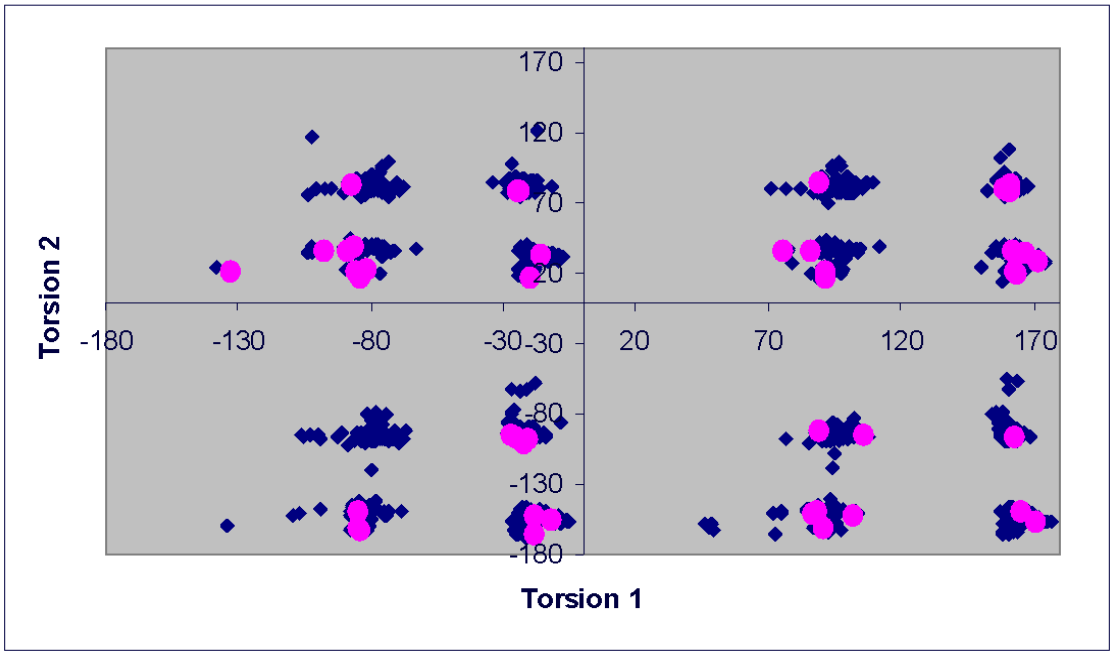

(a)

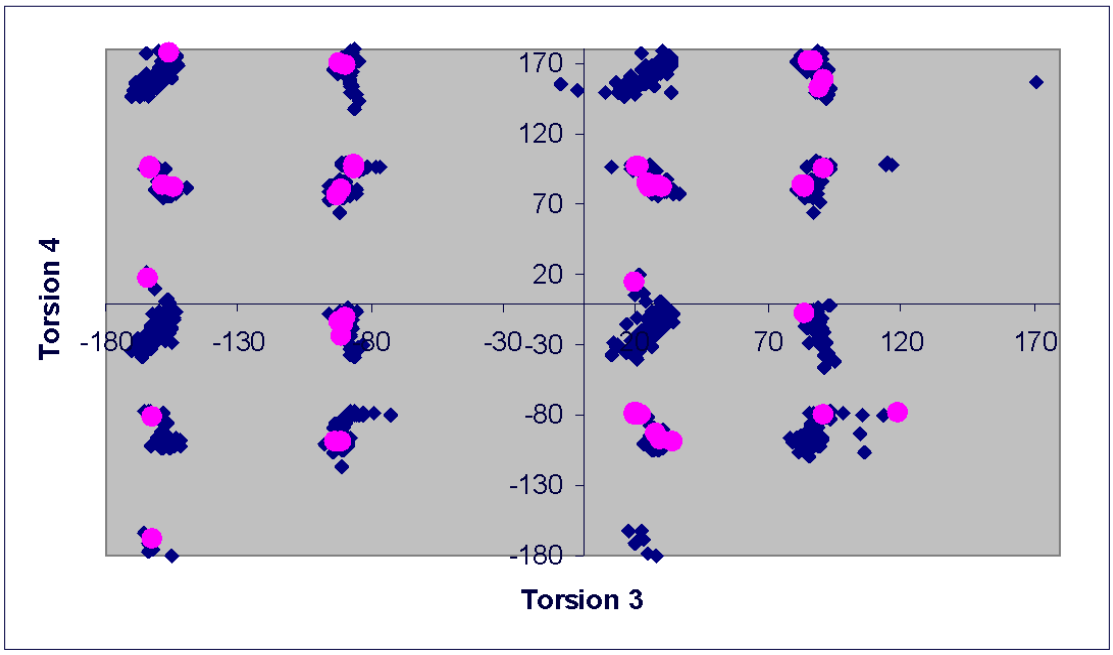

(b)

Figure 21. Plots of Torsion 1 versus Torsion 2 (a) and Torsion 3 versus Torsion 4 (b) for (bppm)Rh(nbd)]$^+$ showing conformational search data points (blue) overlaid with unique data points derived from cClus-A (pink).

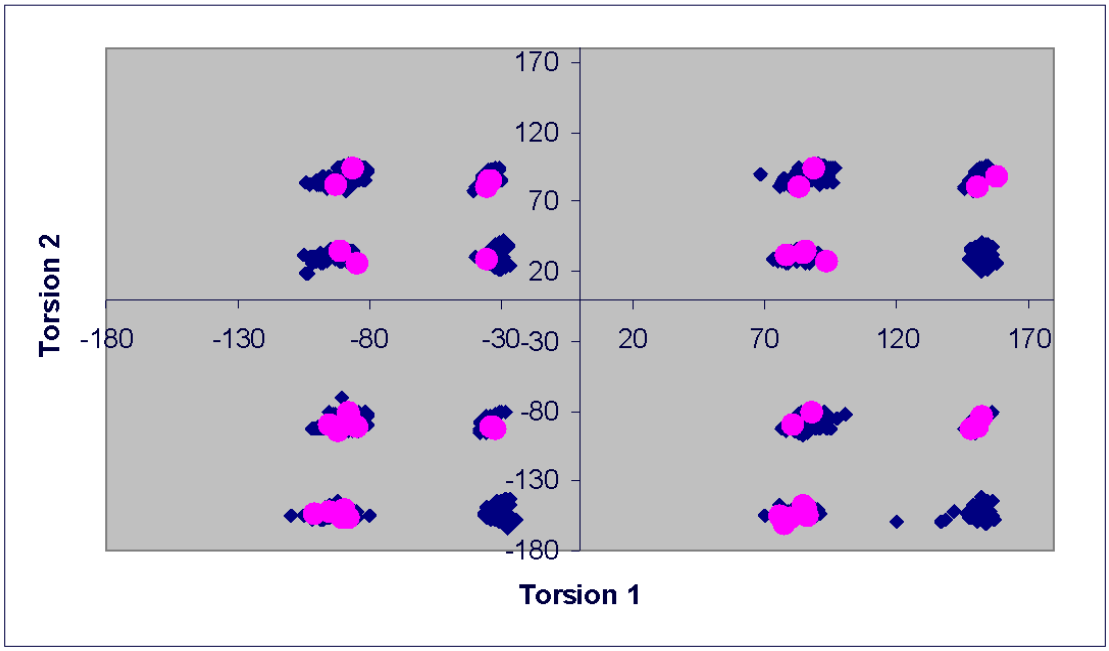

(a)

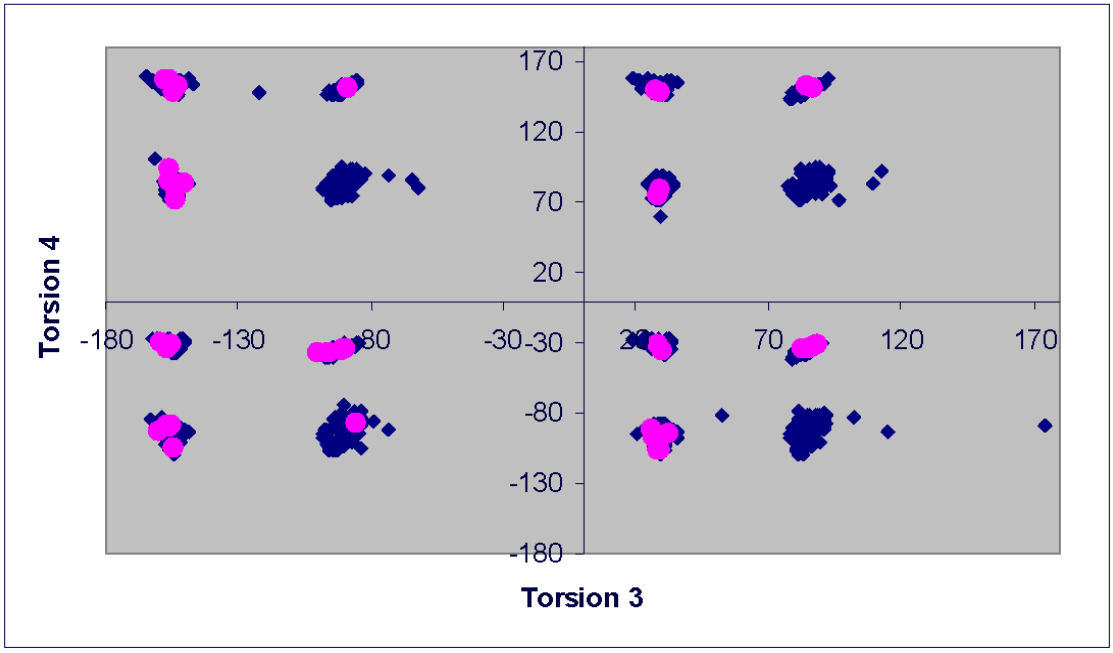

(b)

Figure 22. Plots of Torsion 1 versus Torsion 2 (a) and Torsion 3 versus Torsion 4 (b) for (chiraphos)Rh(nbd)]$^{+}$ showing conformational search data points (blue) overlaid with unique data points derived from cClus-A (pink).

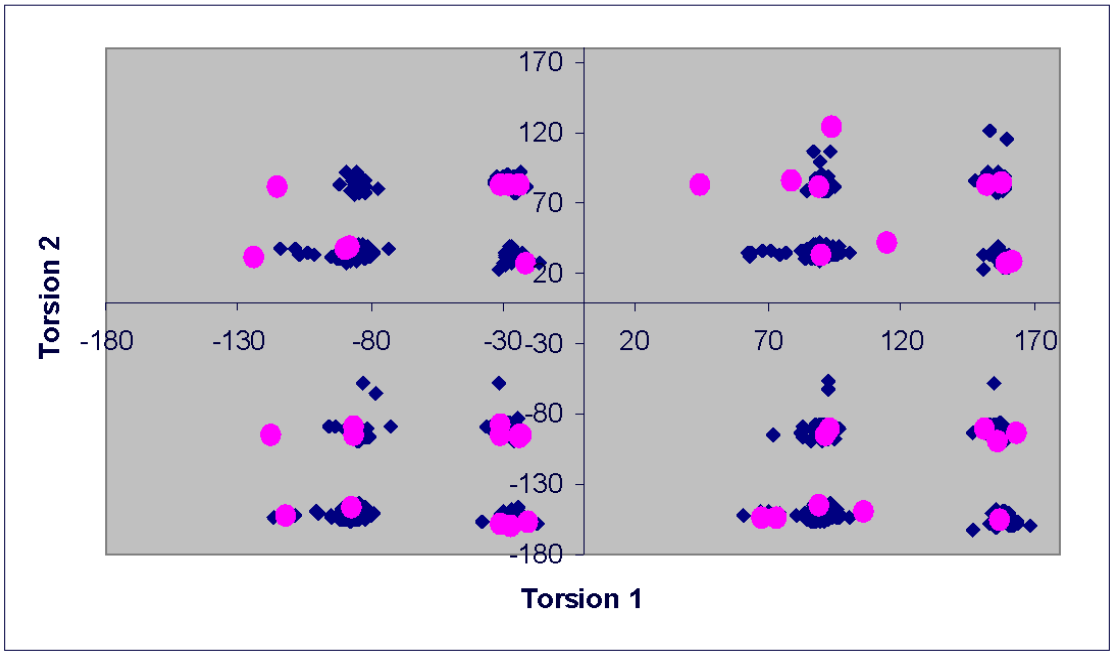

(a)

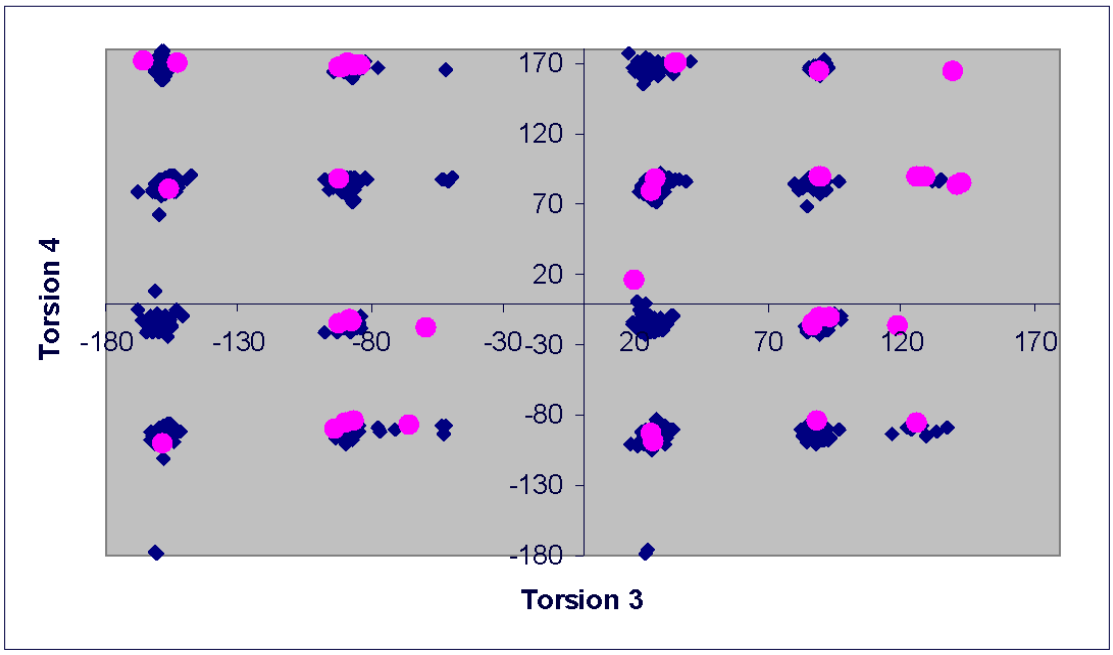

(b)

Figure 23. Plots of Torsion 1 versus Torsion 2 (a) and Torsion 3 versus Torsion 4 (b) for (diop)Rh(nbd)]$^{+}$ showing conformational search data points (blue) overlaid with unique data points derived from cClus-A (pink).

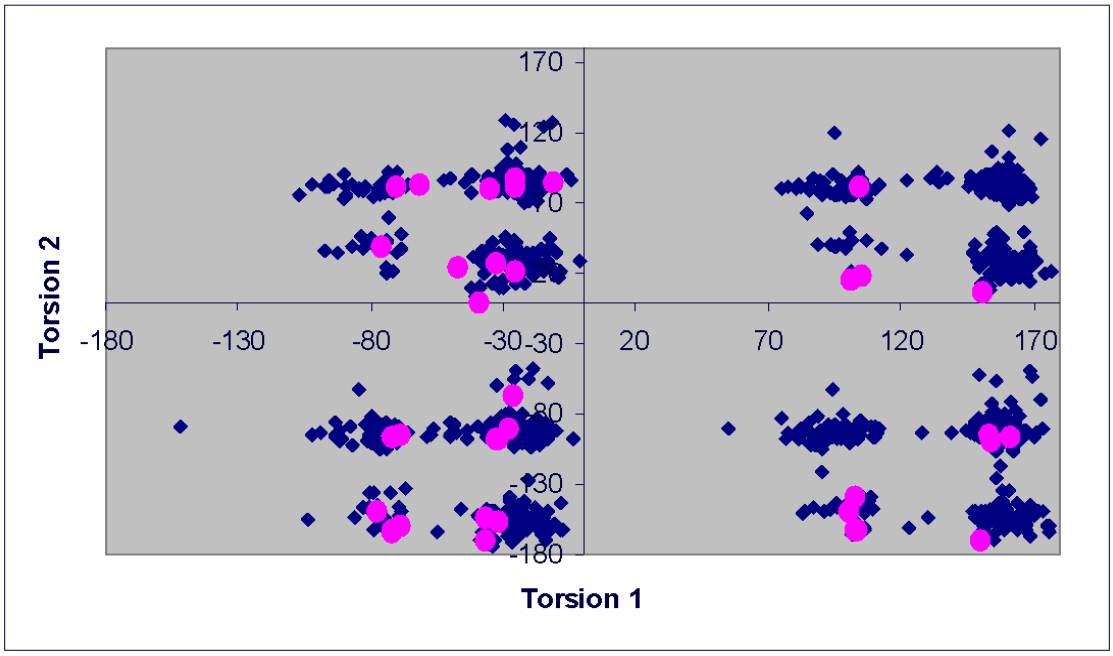

(a)

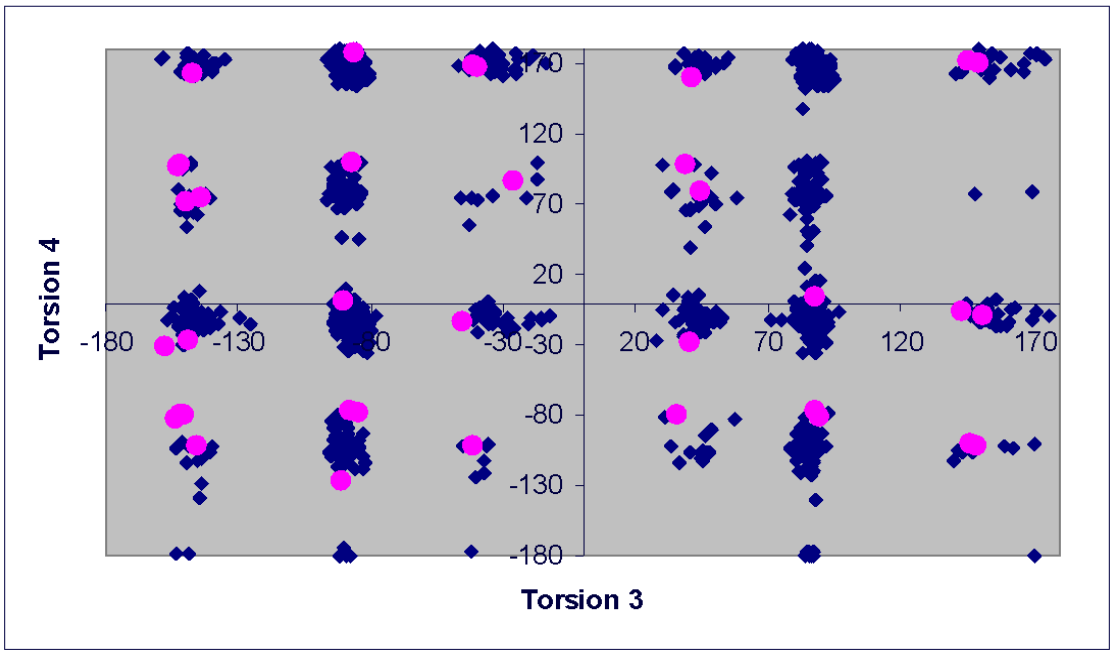

(b)

Figure 24. Plots of Torsion 1 versus Torsion 2 (a) and Torsion 3 versus Torsion 4 (b) for (dmabppm)Rh(nbd)]$^+$ showing conformational search data points (blue) overlaid with unique data points derived from cClus-A (pink).

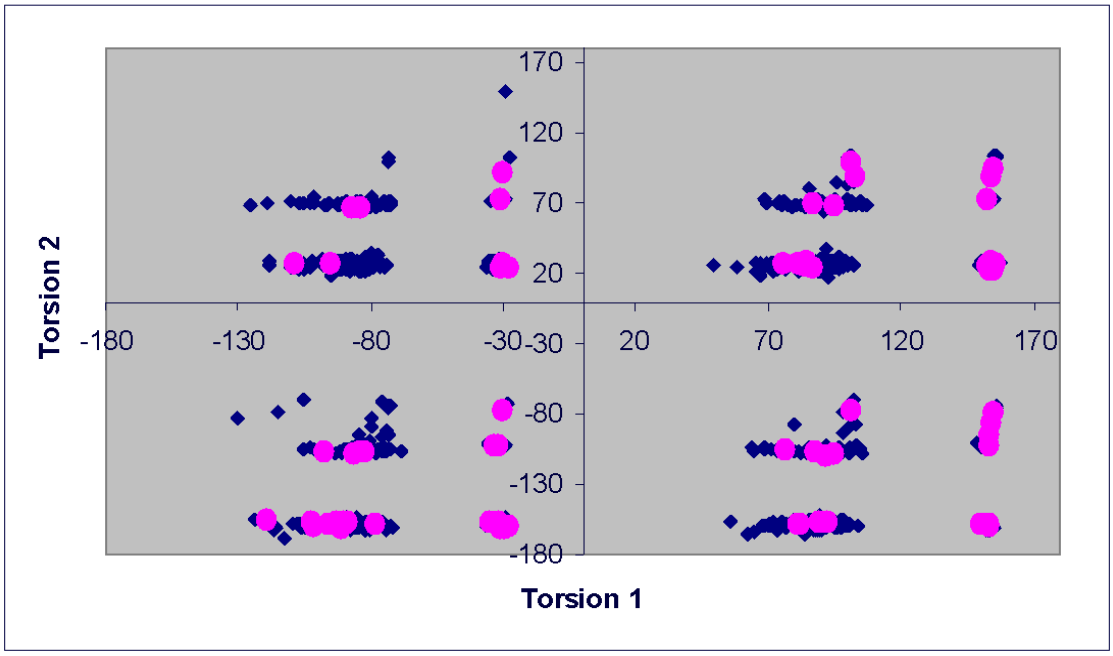

(a)

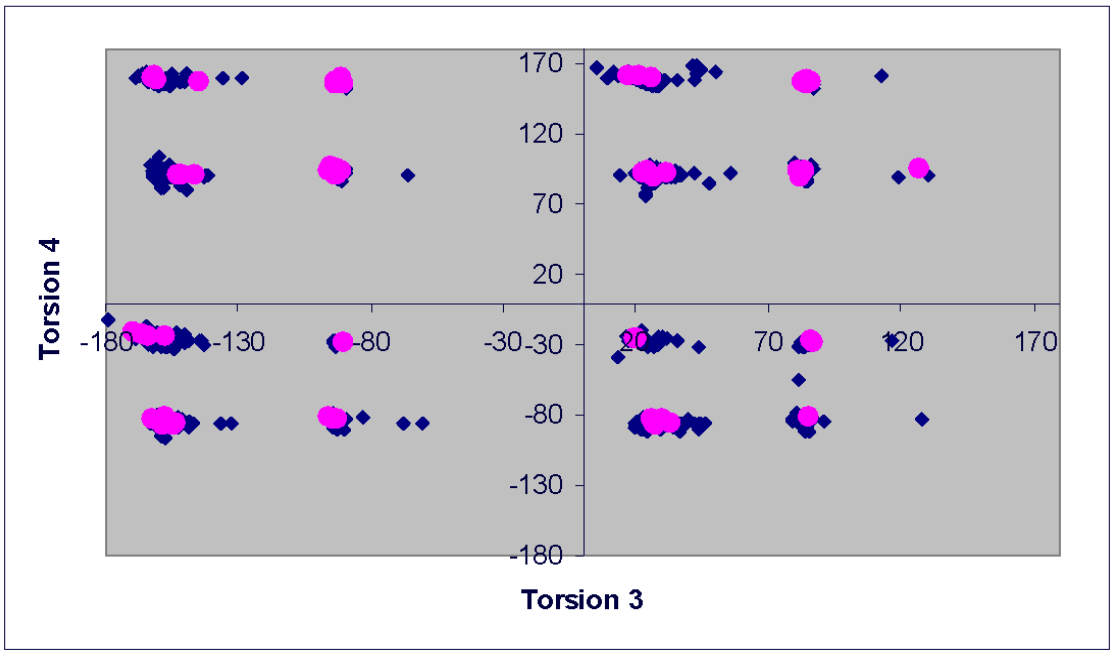

(b)

Figure 25. Plots of Torsion 1 versus Torsion 2 (a) and Torsion 3 versus Torsion 4 (b) for (dpc)Rh(nbd)]$^+$ showing conformational search data points (blue) overlaid with unique data points derived from cClus-A (pink).

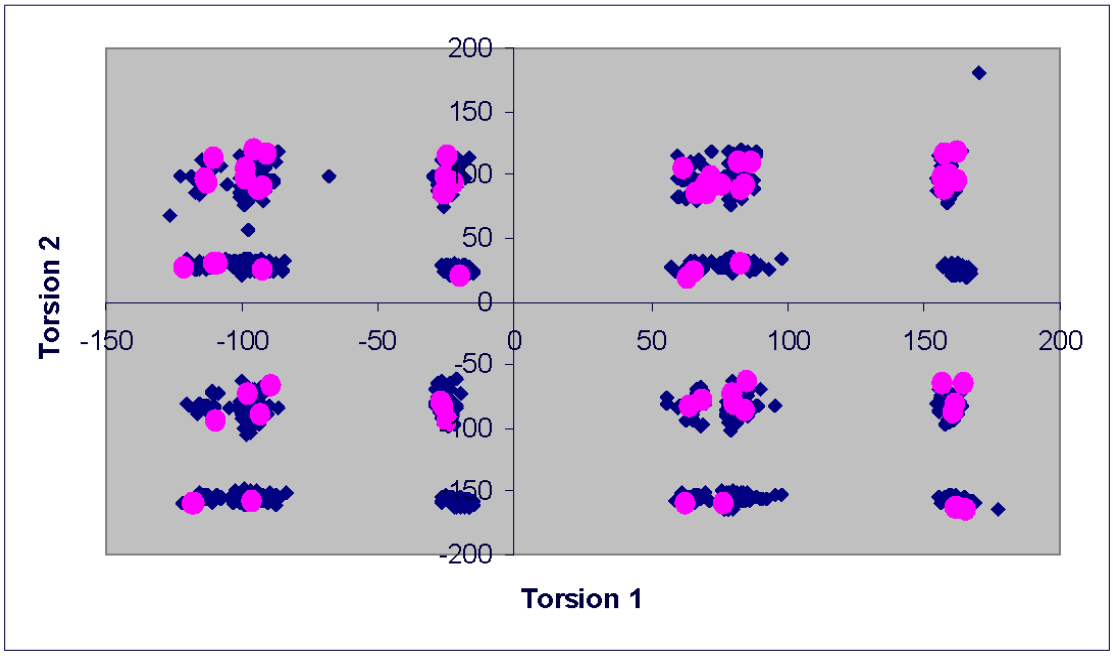

(a)

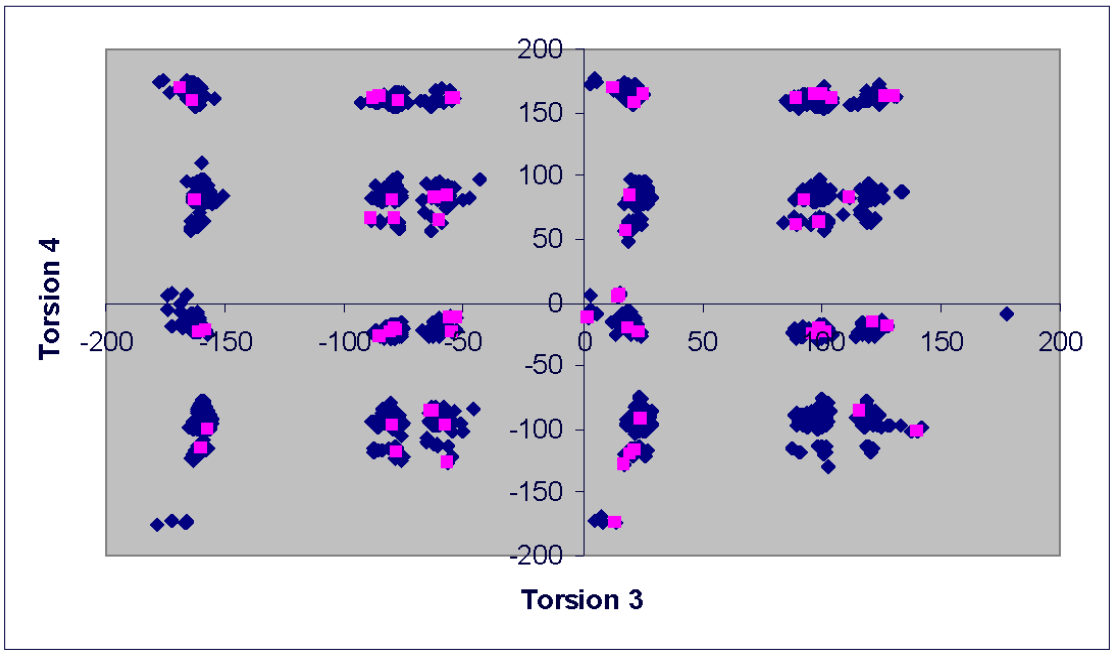

(b)

Figure 26. Plots of Torsion 1 versus Torsion 2 (a) and Torsion 3 versus Torsion 4 (b) for (dpcb)Rh(nbd)]$^+$ showing conformational search data points (blue) overlaid with unique data points derived from cClus-A (pink).

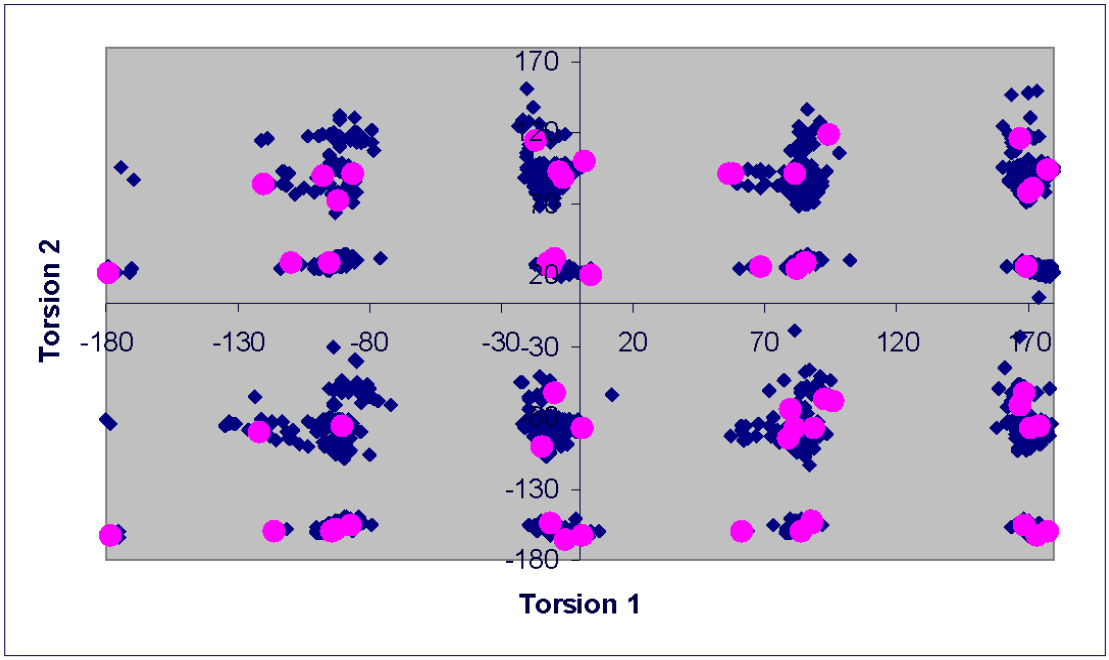
Torsion 2
Torsion 1
170
120
70
20
-30
-130
-180
-180
-130
-80
-30
20
70
120
170

(a)

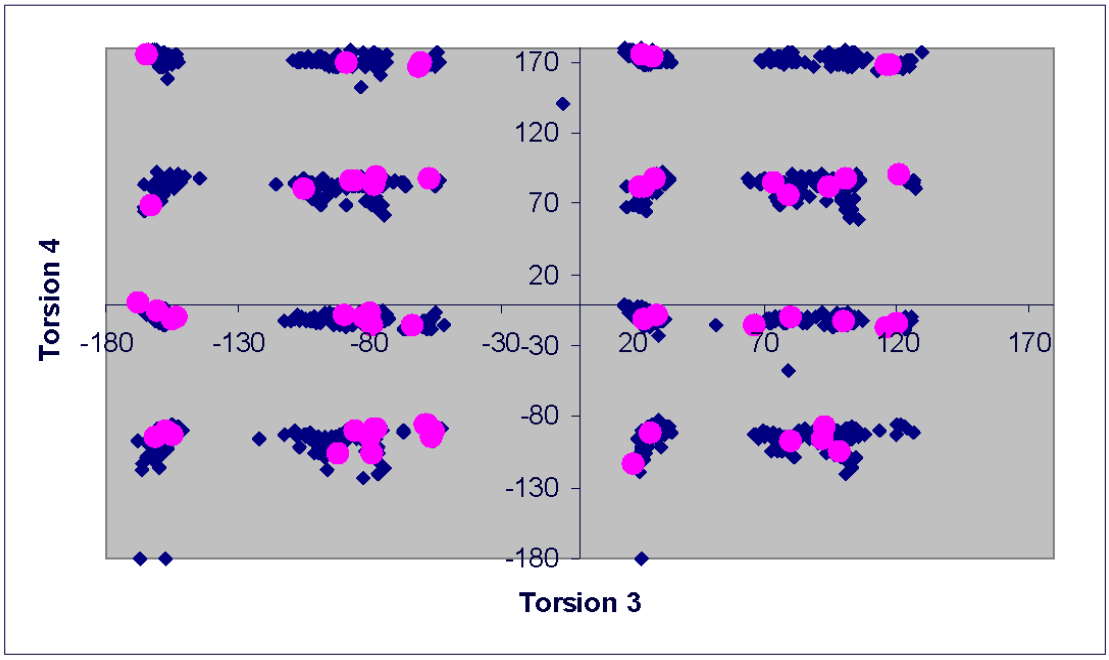

(b)

Figure 27. Plots of Torsion 1 versus Torsion 2 (a) and Torsion 3 versus Torsion 4 (b) for (norphos)Rh(nbd)]$^+$ showing conformational search data points (blue) overlaid with unique data points derived from cClus-A (pink).

REFERENCES

(1) Cotton, F. A.; Wilkinson, G.; Murillo, C. A.; Bochmann, M. *Advanced Inorganic Chemistry*; 6th ed.; Wiley: New York, 1999.

(2) Buda, C.; Burt, S. K.; Cundari, T. R.; Shenkin, P. S. *Inorg. Chem.* 2002, *41*, 2060-2069.

(3) Ball, D. M.; Buda, C.; Gillespie, A. M.; Cundari, T. R.; White, D. P. *Inorg. Chem.* 2002, *41*, 152-156.

(4) Crabtree, R. H. *The Organometallic Chemistry of the Transition Metals*; 3rd ed.; Wiley-Interscience: New York, 2001.

(5) vonZelewsky, A. *Stereochemistry of Coordination Compounds*; Wiley: New York, 1996.

(6) Gillespie, A. M.; White, D. P. *Organometallics* 2001, *20*, 5149-5155.

(7) White, D. P.; Brown, T. L. *Inorg. Chem.* 1995, *34*, 2718-2724.

(8) White, D. P.; Anthony, J. C.; Oyefeso, A. O. *J. Org. Chem.* 1999, *64*, 7707-7716.

(9) Bubel, R. J.; Douglass, W.; White, D. P. *J. Comput. Chem.* 2000, *21*, 239-246.

(10) Burkert, U.; Allinger, N. L. *Molecular Mechanics*; ACS Monograph 177: Washington, D.C., 1982.

(11) Cundari, T. R.; Fu, W. *Inorg. Chim. Acta* 2000, *300 - 302*, 113.

(12) Cundari, T. R., Ed. *Computational Organometallic Chemistry*; Marcell Dekker: New York, 2001.

(13) Gladysz, J. A.; Boone, B. J. *Angew. Chem. Int. Ed. Engl.* 1997, *36*, 550-583.

(14) Brown, T. L. *Inorg. Chem.* 1992, *31*, 1286-1294.

(15) Gillespie, A. M.; White, D. P. *Internet Electron. J. Mol. Des.* 2002, *1*, 23-36, http://www.biochempress.com.

(16) *Cerius*^{2} *4.5*; Accelrys, Inc.: San Diego, CA, 2001.

(17) Rappé, A. K.; Casewit, C. J.; Colwell, K. S.; Goddard, W. A., III; Skiff, W. M. *J. Am. Chem. Soc.* 1992, *114*, 10024-10035.

(18) Spartan version 5.1.3, Wavefunction, Inc. 18401 von Karman Avenue, Suite 370, Irvine, CA 92612 USA.

(19) Cundari, T. R.; Deng, J.; Fu, W. *Intern. J. Quantum Chem.* 2000, *77*, 421-432.

(20) Delley, B. *J. Phys. Chem.* 1990, *92*, 508 -517.

(21) Tsuneda, T.; Suzumura, T.; Hirao, K. *J. Chem. Phys.* 1999, *110*, 10664-10678.

(22) Delley, B. *Int. J. Quantum Chem.* 1998, *69*, 423.

(23) Allen, F. H.; Kennard, O. *Chem. Design Autom. News* 1993, *8*, 31-37.

(24) Choi, M.-G.; Brown, T. L. *Inorg. Chem.* 1993, *32*, 1548-1553.

(25) Choi, M.-G.; Brown, T. L. *Inorg. Chem.* 1993, *32*, 5603-5610.

(26) Choi, M.-G.; White, D.; Brown, T. L. *Inorg. Chem.* 1994, *33*, 5591-5594.

(27) Becke, A. D. *Phys. Rev., B* 1988, *38*, 3098.

(28) Lee, C.; Yang, W.; Parr, R. G. *Phys. Rev., B* 1988, *37*, 785 - 789.

(29) Perdew, J. P.; Chevary, J. A.; Vosko, S. H.; Jackson, K. A.; Peterson, M. R.; Singh, D. J.; Fiolhais, C. *Phys. Rev., B* 1992, *46*, 6671.

(30) Becke, A. D. *J. Chem. Phys.* 1992, *98*, 5648 - 5652.

(31) Frisch, M. J.; Trucks, G. W.; Schlegel, H. B.; Scuseria, G. E.; Robb, M. A.; Cheeseman, J. R.; Zakrzewski, V. G.; MontgomeryJr., J. A.; Stratmann, R. E.; Burant, J. C.; Dapprich, S.; Millam, J. M.; Daniels, A. D.; Kudin, K. N.; Strain, M. C.; Farkas, O.; Tomasi, J.; Barone, V.; Cossi, M.; Cammi, R.; Mennucci, B.; Pomelli, C.; Adamo, C.;

Clifford, S.; Ochterski, J.; Petersson, G. A.; Ayala, P. Y.; Cui, Q.; Morokuma, K.; Malick, D. K.; Rabuck, A. D.; Raghavachari, K.; Foresman, J. B.; Cioslowski, J.; Ortiz, J. V.; Baboul, A. G.; Stefanov, B. B.; Liu, G.; Liashenko, A.; Piskorz, P.; Komaromi, I.; Gomperts, R.; Martin, R. L.; Fox, D. J.; Keith, T.; Al-Laham, M. A.; Peng, C. Y.; Nanayakkara, A.; Challacombe, M.; Gill, P. M. W.; Johnson, B.; Chen, W.; Wong, M. W.; Andres, J. L.; Gonzalez, C.; Head-Gordon, M.; Replogle, E. S.; Pople, J. A. *Gaussian 98, Revision A.9* Pittsburgh, PA, 1998.

(32) Maseras, F. In *Computational Organometallic Chemistry*; Cundari, T. R., Ed.; Marcel Dekker: New York, 2001, pp 159-184.

(33) Svenson, M.; Humbel, S.; Froese, R. D. J.; Matsubara, T.; Sieber, S.; Morokuma, K. *J. Phys. Chem.* 1996, *100*, 19357.

(34) Dapprich, S.; Komáromi, I.; Byun, K. S.; Morokuma, K.; Frisch, M. J. *J. Mol. Struct. (Theochem)* 1999, *461*, 21.

(35) Gillespie, A. M.; Morello, G. R.; White, D. P. *Organometallics* 2002, *21*, 3913-3921.

(36) Hegedus, L. S. *Transition Metals in the Synthesis of Complex Organic Molecules*; 2 ed.; University Science Books: Sausalito, CA, 1999.

(37) Kagan, H. B.; Dang, T.-P. *J. Am. Chem. Soc.* 1972, *94*, 6429-6433.

(38) Fryzuk, M. D.; Bosnich, B. *J. Am. Chem. Soc.* 1977, *99*, 6262-6267.

(39) Vineyard, B. D.; Knowles, W. S.; Sabacky, M. J.; Bachman, G. I.; Weinkauff, D. J. *J. Am. Chem. Soc.* 1977, *99*, 5946-5952.

(40) Knowles, W. S. *Accts. Chem. Res.* 1983, *16*, 106.

(41) Tye, H. *J. Chem. Soc., Perkin Trans. 1* 2000, 275-298.

(42) Peng, T.-S.; Pu, J.; Gladysz, J. A. *Organometallics* 1994, *13*, 929-940.

(43) Boone, B. J.; Klein, D. P.; Seyler, J. W.; Méndez, N. Q.; Arif, A. M.; Gladysz, J. A. *J. Am. Chem. Soc.* 1996, *118*, 2411-2421.

(44) Kolb, H. C.; VanNieuwenhze, M. S.; Sharpless, K. B. *Chem. Revs.* 1994, *94*, 2483-2547.

(45) Becker, H.; Soler, M. A.; Sharpless, K. B. *Tetrahedron* 1995, *51*, 1345-1376.

(46) Veldkamp, A.; Frenking, G. *J. Am. Chem. Soc.* 1994, *116*, 4937-4946.

(47) Palucki, M.; Pospisil, P. J.; Zhang, W.; Jacobsen, E. N. *J. Am. Chem. Soc.* 1994, *116*, 12135.

(48) Palucki, M.; McCormick, G. J.; Jacobsen, E. N. *Tetrahedron Lett.* 1995, *36*, 5457-5460.

(49) Larrow, J. F.; Schaus, S. E.; Jacobsen, E. N. *J. Am. Chem. Soc.* 1996, *118*, 7420-7421.

(50) Jacobsen, E. N. In *Catalytic Asymmetric Synthesis*; Ojima, I., Ed.; VCH: New York, 1993, pp 159-202.

(51) Casalnuovo, A. L.; RajanBabu, T. V.; Ayers, T. A.; Warren, T. H. *J. Am. Chem. Soc.* 1994, *116*, 9869-9882.

(52) Inoguchi, K.; Sakuraba, S.; Achiwa, K. *Synlett* 1992, 169-178.

(53) Landis, C. R.; Root, D. M.; Cleveland, T. In *Reviews in Computational Chemistry*; Lipkowitz, K. B., Boyd, D. B., Eds.; VCH: New York, 1995; Vol. 6, pp 73-381.

(54) Comba, P.; Hambley, T. W. *Molecular Modeling of Inorganic Compounds*; VCH: New York, 1995.

(55) Rappé, A. K.; Casewitt, C. J. *Molecular Mechanics Across Chemistry*; University Science Books: Sausalito, 1997.
(56) Landis, C. R.; Hilfenhaus, P.; Feldgus, S. *J. Am. Chem. Soc.* 1999, *121*, 8741-8754.
(57) Feldgus, S.; Landis, C. R. *J. Am. Chem. Soc.* 2000, *122*, 12714-12727.
(58) Lipkowitz, K. B. *J. Chromatogr. A* 1994, *666*, 493-503.
(59) Aerts, J. *J. Comput. Chem.* 1995, *16*, 914-922.
(60) McDonald, D. Q.; Still, W. C. *J. Am. Chem. Soc.* 1996, *118*, 2073-2077.
(61) McDonald, D. Q.; Still, W. C. *J. Am. Chem. Soc.* 1994, *116*, 11550-11553.
(62) Brunner, H. In *Topics in Stereochemistry*; Interscience: New York, 1988; Vol. 18, p 129.
(63) Caffery, M. L.; Brown, T. L. *Inorg. Chem.* 1991, *30*, 3907-3914.
(64) Lee, K. J.; Brown, T. L. *Inorg. Chem.* 1992, *31*, 289-294.
(65) Brown, T. L.; Lee, K. J. *Coord. Chem. Rev.* 1993, *128*, 89-116.
(66) Giovannetti, J. S.; Kelly, C. M.; Landis, C. R. *J. Am. Chem. Soc.* 1993, *115*, 4040-4057.
(67) Although the phenyl group torsions are modulo 180, the molecular mechanics program requires that the search window extend over 360 to ensure unbiased coverage of the entire torsional space. This means that the resulting plots are redundant in each torsional dimension, to the extent that the coverage is sufficient to properly represent the surface. In effect, the unique quadrant in each 2D plot. In comparing torsional angle values, it is useful to recall that phenyl group rotations are modulo 180 . Thus, a value of -85 is equivalent to +95 ; a value of -155 is equivalent to +25 .
(68) Brown, J. M.; Evans, P. L. *Tetrahedron* 1988, *44*, 4905-4916.
(69) Freeze, M.; Morello, G.; White, D. P. *J. Comput. Chem.* Submitted, 2003.